Instructive Roles of Acetylated Histone Marks at Mouse Meiotic Recombination Hotspots

Irina V. Getun,[a#], Zhen Wu,[a] Mohammad Fallahi,[a,b] Souad Ouizem,[c] Qin Liu,[c*] Weimin Li,[a] Roberta Costi,[d] William R. Roush,[c] John L. Cleveland,[a**##] and Philippe R. J. Bois[a***]**

Department of Cancer Biology, The Scripps Research Institute, Jupiter, Florida, USA[a]; Informatics Core, The Scripps Research Institute, Jupiter, Florida, USA[b]; Department of Chemistry, The Scripps Research Institute, Jupiter, Florida, USA[c]; Dipartimento di Chimica e Tecnologie del Farmaco, Istituto Pasteur-Fondazione Cenci Bolognetti, "Sapienza" Università di Roma, Roma, Italy[d]

Running Head: Histone acetylation controls meiotic DSB

[#]Address correspondence to Irina V. Getun, igetun@scripps.edu.
[##]Address correspondence to John L. Cleveland, John.Cleveland@moffitt.org.

*Present address: School of Pure and Applied Science, Florida Southwestern State College, Fort Myers, Florida, USA.
**Present address: Department of Tumor Biology, The Moffitt Cancer Center and Research Institute, Tampa, Florida, USA.
***Present address: Avespa, Miami, Florida, USA.

ABSTRACT

Meiotic recombination initiates following the formation of DNA double strand breaks (DSBs) by the Spo11 endonuclease at the leptotene stage of meiosis I at discrete regions in the genome coined hotspots. In mammals, meiotic DSB site selection is directed in part by sequence specific binding of PRDM9, a polymorphic histone H3 methyltransferase. However other chromatin features needed for meiotic hotspot specification are largely unknown. Here, we show that the recombinogenic cores of active hotspots harbor several histone H3 and H4 acetylation and methylation marks that are typical of open, active chromatin. Further, deposition of these histone marks is dynamic and manifest at pre-leptotene meiotic cells, which would facilitate the formation of DSBs at leptotene. Importantly, manipulating histone acetylase and deacetylase activity established that histone acetylation marks are necessary for both hotspot activity and crossover resolution. We conclude there are instructive roles for histone acetylation at mammalian meiotic recombination hotspots**.**

INTRODUCTION

The chromatin features and regulatory factors that control mammalian meiotic DSB site selection, initiation, crossover (CO) activity and resolution are poorly understood. Histone modifications, including acetylation, methylation and ubiquitination, have been suggested to affect meiotic recombination in yeast and higher eukaryotes (1-7). Specifically, select histone modification enzymes, including histone acetyltransferases, deacetlyases and methyltransferases, have been shown to have roles in regulating meiotic double strand breaks (DSBs) in *C. elegans* and yeast, by controlling the conformation of chromatin around recombination hotspots (5, 8-13). Further, in mice, a hallmark histone modification of meiotic hotspots is trimethylated lysine-4 of histone H3 (H3K4Me3), which is directed by the highly polymorphic histone methyltransferase PRDM9 (3, 14-19) and which is present in at least 87% of hotspots (3). Finally, H3K4Me3, H3K4Me2 and H3K9Ac marks have been suggested to be important for the initiation of meiotic recombination at the *Psmb9* hotspot in mice, while histone H4 hyperacetylation has been shown to be a feature of the mouse *Hlx1* hotspot core during meiotic DSB repair (2).

At this juncture it is unclear if there are dynamic and select changes in histone modifications at mouse recombination hotspots throughout meiosis and if such marks play instructive or passive roles in the control of recombination. Using highly purified fractions of cells from all stages of meiosis I and native chromatin immunoprecipitation (nChIP)/real-time PCR profiling, here we report that there are dynamic changes in acetylated and methylated histone marks found in open chromatin at recombinogenically active meiotic hotspot cores, and that specifically histone acetylation plays profound

instructive and necessary roles in laying down histone methylation marks and in hotspot crossover activity.

MATERIALS AND METHODS

Mouse strains. Mice were bred and maintained at the Animal Resource Center facility of The Scripps Research Institute-Scripps Florida under the Institutional Animal Care and Use Committee guidelines and an IACUC-approved protocol. Mice strains C57Bl/6J, DBA/2J, CAST/EiJ and C57Bl/6JxDBA/2J F1 males (B6D2F1/J) were purchased from the Jackson Laboratory (Bar Harbor, ME). *Spo11*$^{+/-}$ breeding pairs were generously provided by Dr. R. Daniel Camerini-Otero (NIDDK/NIH, Bethesda, MD).

Dissociation of testis cells and FACS sorting. Spermatogonia, pre-leptotene, leptotene/zygotene and pachytene/diplotene cell fractions were purified as described (20, 21). Briefly, C57Bl/6JxDBA/2J F1 or CAST/EiJxDBA/2J F1 meiotic cells fractions (hereafter B6 for C57Bl/6J, DBA for DBA/2J and CAST for CAST/EiJ) were purified using a FACS-based method (20, 21). Sorting was performed on a Becton-Dickinson Aria cell sorter as described (21). Sorts were typically 3-6 hr to collect 0.2-1.0x10^6 cells for each population with more than 95 % purity for pre-leptotene, leptotene-zygotene and pachytene-diplotene cells (20). Usually two to four testes were processed per sort.

Sample collection, RNA extraction and array hybridization of *Spo11*$^{-/-}$ meiotic cells.

Spermatogonia, pre-leptotene and leptotene/zygotene sorted meiotic fractions were collected from 10 to 16 weeks old *Spo11*$^{-/-}$ mouse testes. RNA was extracted from sorted cells as described (22). Each independent RNA pool included cells from two sorts of meiotic cells from a total of 4 and 3 *Spo11*$^{-/-}$ mice testes, respectively, which were combined for microarray hybridizations. RNA labeling and microarray hybridizations to MOE430v2.0 arrays (Affymetrix) were performed as described (22).

Microarray analysis of histone modifying enzymes during meiosis in wild type and *Spo11*$^{-/-}$ mice. Initial analysis for C57Bl/6JxDBA/2J F1 mouse meiotic samples has been described (22), GEO accession number GSE21447. Here, 3 meiotic *Spo11*$^{-/-}$ cell samples (spermatogonia, pre-leptotene and leptotene/zygotene) and 8 meiotic wild-type B6/DBA cell samples (spermatogonia, pre-leptotene, leptotene/zygotene, early pachytene, mid pachytene, late pachytene, diplotene and round spermatids), or a total of 23 Affymetrix Mouse430v2.0 CEL files, were analyzed using GeneSpring GX v12.1. The summarization algorithm was set to GCRMA. Quantile normalization was applied and the baseline transformation was set to the median of all samples. Replicate samples were grouped for each cell type. GeneSpring GX GO analysis function was used to identify genes (probe sets) with histone acetylases, histone deacetylases, histone methylases and histone demethylases activities. Probe sets with signal higher than Chip median in one cell type or more were analyzed. To generate the heatmaps for each gene list (Figs. 1 and 7), the GeneSpring GX hierarchical clustering algorithm was utilized. In all heatmaps an absolute fold change filter of 1.5-fold for spermatogonia/average pachytene expression ratio was applied to obtain the differentially expressed gene list followed by hierarchical clustering.

The gene expression data for secondary spermatids stage were omitted. Only significantly changed probe sets with p-value (corrected) <0.05 are shown. Microarray data were normalized across the median of all 11 *Spo11*$^{-/-}$ and wild type cell type samples. Statistical analysis details are provided in Table A1 of the Appendices. The combined microarray dataset is available in the Gene Expression Omnibus (GEO) database (http://www.ncbi.nlm.nih.gov/gds), accession number GSE57197.

Quantitative RT-PCR. Total RNA was isolated from the sorted spermatogonia, pre-leptotene, leptotene/zygotene and pachytene/diplotene meiotic cell fractions as described (22). cDNAs were generated using iScript™ cDNA Synthesis Kit (Bio-Rad) and were quantified with Quant-iT™ OliGreen® ssDNA Assa Kit (Invitrogen). Real-time PCR primers for qRT-PCR analyses of genes encoding HATs and HDACs (Fig. 1C) were designed using Primer3 software (http://www.frodo.wi.mit.edu/primer3/) for intronic or cross intron/exon boundaries of a gene to yield a short (200–250 bp) PCR fragments with a melting temperature of about 60°C (see Table A2 in the Appendices). Primers pairs used for qRT-PCR analyses of specific meiotic stage marker genes (Fig. 1D) were as described (23). For each reaction, 0.9 ng of cDNA was mixed with 2.5 pmol of each primer in 5 µl (final volume) of SYBR Green Master Mix (Quanta Biosciences) and ROX dye (Invitrogen) as a reference. All amplifications were run in triplicate.

Preparation of mono-nucleosomes by micrococcal nuclease (MNase) digestion of native chromatin. Mono-nucleosomes were isolated from native chromatin of B6xDBA F1, CASTxDBA F1 or *Spo11*$^{-/-}$ mouse meiotic cells as described (20), with minor

modifications. In addition to protease inhibitor cocktail (Roche), all cell processing solutions were supplemented with 10 mM Na-butyrate when performing native ChIP analyses of acetylated histone marks. After MNase digestion and the first round of nucleosome extraction to S1 supernatant, the remaining chromatin pellet was resuspended in 200-µL of lysis buffer (LB: 10 mM Tris pH 7.5, 10 mM NaCl, 3 mM $MgCl_2$, 0.4 % NP-40, 1mM $CaCl_2$, 0.25 mM EDTA), kept on ice and slightly sonicated in water bath at 4°C. Sonication was performed on a Misonix Sonicator 3000 at power level 5 for 1 min followed by 1 min pause for 120 sec of the total sonication time. The suspension was centrifuged for 10 min at 10,000 rpm at 4°C, the supernatant retained (supernatant "S2") and processed as described (20).

Native ChIP of histone modification marks. Immunoprecipitations following the preparation of mono-nucleosomes from native chromatin were performed using protein G agarose (Millipore) as described for native histone H3 ChIP (20). The following antibodies were used for ChIP analyses: H4K12Ac (Abcam, ab1761, ab46983 and Active Motive, #39927); H4K5Ac (Abcam, ab1758); H4K8Ac (Abcam, ab15823); H4K16Ac (Millipore, #06-762 and Abcam, ab61240); H4K91Ac (Abcam, ab4627); H3K9Ac (Abcam, ab12179); H3K4Me3 (Millipore, #07-473 and Abcam, ab8580); H3K4Me2 (Millipore, #07-030); H3K79Me1 (Abcam, ab2886); H3K36Me3 (Abcam, ab9050); H4K20Me3 (Abcam, ab9053); H4K20Me1 (Abcam, ab9051); H4K20Me2 (Millipore, #07-367); H3K9Me3 (Abcam, ab8898); H3K27Me3 (Cell Signaling, #9756); and H3K9/K14Ac (Pierce, # PA5-16194).

Briefly, 0.2-1.0x10^6 B6xDBA F1, CASTxDBA F1 or *Spo11*$^{-/-}$ meiotic cells were isolated by FACS. Typically 2-4 µg of an antibody was incubated with chromatin. As a control, no

156 antibody ChIP was performed. DNA from input and bound ChIP fractions was isolated as
157 described (20), quantified using PicoGreen kit (Invitrogen) and used for real-time PCR
158 analysis.
159
160 **Real-time PCR and data analysis.** Real-time PCR and data analysis was performed as
161 described (20). In brief, to define histone modification profiles across the four mouse
162 recombination hotspots studied, we used primer pair tiling across the selected loci, using
163 70–140 bp amplicons centered on average every 30–75 bp (20) (see Fig. A1 in the
164 Appendices). Primer pairs used to tile *HS22, HS59.4* and *HS61.1* hotspots were as described
165 (20); the *HS59.5* real-time PCR primers are provided in Table A3 of the Appendices. All
166 real-time PCR quantifications were performed using a Mastercycler RealPlex4S
167 (Eppendorf) using SYBR Green fluorescence (Quanta Biosciences) and ROX dye
168 (Invitrogen) as a reference and the real-time PCR conditions as described previously (20).
169 The position at the center of each amplicon was used as the abscissa value for points
170 plotted across the hotspots histone modification maps. All initial histone modification
171 profiles (in Figs. 2-6, 9A and 9C, in Figs. S1, S3 and the histone H3K4Me3 profiles in Fig.
172 S2A) were calculated as the absolute fold enrichment using the $2^{-\Delta Ct}$ formula, with
173 $\Delta Ct=Ct^{IP(Bound)}-Ct^{(Input)}$. We used arbitrary Ct cut-off values of above 31 and 29 for Input and
174 IP Bound DNA, respectively. For $2^{-\Delta Ct}$ enrichment calculations, a value above 0.15 was
175 considered as significant. A profile for every histone mark was obtained after averaging
176 enrichment curves from at least two independent ChIP experiments. No antibody ChIP
177 profiles were averaged by all the meiotic stages. The normalized native ChIP profiles that
178 are shown in Figs. 2-6, 9A and 9C, and in Figs. S1 and S3, were obtained by $2^{-\Delta\Delta Ct}$

normalization, where ΔΔCt = ΔCT ChIP1(histone mark ChIP, CAST/DBA, *Spo11*$^{-/-}$ or s2-, 2c treated) - ΔCT ChIP2(no antibody control ChIP, B6/DBA or vehicle treated).

Solexa sequencing of mono-nucleosomal DNA. Mono-nucleosomal DNA was isolated from total meiotic populations of 10-week old B6 male testes (1.3 x 10^6 cells) by MNase digestion of native chromatin as described (20) (see Fig. S2B). Final mono-nucleosomal DNA was purified using phenol/chloroform extraction followed by ethanol precipitation (20), run on 2 % agarose gel and isolated using Qiagen gel extract kit (see Fig. S2C). For whole-genome sequencing, nucleosomal DNA was further ligated to adaptors, amplified using Solexa primers following the Illumina sequencing protocol and sequenced with an Illumina GAII Genome Analyzer. We obtained approximately 140 million reads of 75 nucleotides (nt) with about 73 million reads that were uniquely mapped to mouse genome (mm9, University of California, Santa Cruz (UCSC) genome database). A combined bed file with aligned reads was downloaded to Integrative Genomic Viewer software (IGV 2.3) for visualization.

Identification and crossover analysis of *HS59.5* recombination hotspot on mouse chromosome 19. The *HS22*, *HS59.4* and *HS61.1* hotspots have been described (20, 24, 25). The *HS59.5* hotspot was identified using similar allele-specific PCR strategy (24, 25). In brief, SNP analysis was performed in BXD recombinant inbred lines followed by two rounds of allele-specific oligonucleotide (ASO) amplification of isolated B6xDBA F1 sperm (24, 25). All PCR reactions were performed with the reaction buffer described (24, 26). Amplifiable molecules were determined using Poisson analysis (24). For the *HS59.5*

hotspot, DNA was digested with the *XhoI* restriction enzyme to cleave outside the tested intervals. Both B6-to-DBA and DBA-to-B6 CO orientations were analyzed. SNPs are indicated in bold. For the B6xDBA F1 sperm DNA, *HS59.5* 5' allele specific primers were 59.5DBAF1.3 (5'-GG**C** AAC TGA AAT CAA ATA CA**C**-3') and 59.5DBAF2.3 (5'-GA**C** TGG AAA ACC ATT CCA TTC **C**A**T**-3') for DBA, 59.5B6F1.3 (5'-GG**T** AAC TGA AAT CAA ATA CA**T** G-3') and 59.5B6F2.3 (5'-CGG A**A**T GGA AAA CCA TTC **T**A**C**-3') for B6. The 3' primers were 59.5DBAR1.3 (5'-TTG GAA TTC AAG AAC AAA **T**A**C**-3') and 59.5DBAR2.3 (5'-CTG CAC AGT AAG TCC AG**G T**-3') for DBA and 59.5B6R1.3 (5'-TTG GAA TTC AAG AAC AAA **C**A**G**-3') and 59.5B6R2.3 (5'-GTG CAC AGT AAG TCC AG**T G**-3') for B6. The first round was performed using the 59.5 F1.3 and 59.5 R1.3 primer pair (6.9 kb), and the second round with the 59.5 F2.3 and 59.5 R2.3 primer pair (6.5 kb). The first round of PCR reactions were performed at 94°C for 1 min followed by 28 cycles at 94°C for 30 sec, 54°C for 45 sec, and 63°C for 6 min. The second round of PCR reactions were performed at 94°C for 1 min followed by 30 cycles at 94°C for 30 sec, 54°C for 45 sec, and 63°C for 6 min.

All primary PCR products were digested with S1 nuclease to remove single-stranded DNA as described (24, 26). Secondary PCR reactions were seeded with 100-fold diluted S1-treated DNA. Secondary PCR products (70% of total reaction volume) were run on 0.8% agarose gels in 0.5 X TBE and visualized by staining with ethidium bromide and UV light. DNA inputs per small-pool PCR reaction consisted of ~1,000 amplifiable molecules. This was equivalent to 0.2 to 0.4 recombinant molecules per pool. We typically obtained 10% to 30% positive pools per experiment, to limit reactions with two recombinant molecules. All recombinant molecules were sequenced and analyzed using the Sequencher software (v4.9, GeneCodes). *HS59.5* sequencing primers were HS59.5F11 (5'-ACC GAC TGT GTG TGT GTG

TGT-3'), HS59.5F12 (5'-GCT TCT ACA CCT GCC ACA ACT-3'), HS59.5F13 (5'-GGA GCA CAT CCA CAC TTC TGT-3'), HS59.5R11 (5'-AGA CCC ACA AAC AGC ACT GAG-3'), HS59.5R12 (5'-GAA GGA TGT CAC CAT GTC ACC-3'), and HS59.5R13 (5'-AAT CAG AAC ATG GCC TCC TG-3'). Recombination rates and 95 % confidence intervals were calculated as described (24, 25) (Table A4 in the Appendices). The CO profile for the *HS59.5* hotspot has been described (10).

Synthesis of HDAC and HAT inhibitors. The 4-dimethylamino-*N*-[5-(2-mercaptoacetylamino)-pentyl]-benzamide (s2) HDAC inhibitor and the 2,6-Bis(3-bromo-4-hydroxybenzylidene)cyclohexanone (2c) HAT inhibitor were synthesized as described (27, 28).

Preparation of liposomal 2c compound. The 2c drug has poor solubility in water and when used in DMSO solution was toxic. Therefore, based on the similarity of the structures of 2c and curcumin, we adapted a protocol developed for liposome-encapsulated curcumin (29, 30) to prepare liposomal 2c drug soluble in saline. In brief, 1,2-dimyristoyl-sn-glycero-3-phosphocholine (DMPC) and 1,2-dimyristoyl-sn-glycero-3-phospho-rac-(1-glycerol) (DMPG) lipids (Avanti Polar Lipids) in 9:1 ratio were dissolved in tert-butanol at a concentration of 10 mg/mL. Sterile water (1/20 volume) and one part 2c compound were added for a final lipid/2c ratio of 10:1. The solution was sterile-filtered, frozen in dry ice and ethanol, and lyophilized overnight. The modified drug was soluble in saline up to 10 mg/ml and had no toxicity in treated male mice.

HDAC and HAT *in vivo* inhibitor studies. Our small compound treatment strategy takes advantage of the linear process of meiosis I, where an acute drug treatment (typically 5 to 10 days) will affect early mouse meiotic cells at a set time, and where consequences are then assessed via analyses of sperm DNA. Inhibitors were administered to 10 week-old mice daily for 5 (2c-HAT inhibitor) or 8 (s2-HDAC inhibitor) days by *i.p.* injection; vehicle was injected to a control cohort of male mice. Doses for s2 inhibitor treatment were as described (31). The dosage of the 2c HAT inhibitor used *in vivo* was validated in this study. A group of 8 mice were treated. S2 compound was resuspended in DMSO (0.25 %)/sterile 0.9% NaCl vehicle and was injected *i.p.* daily (1mg/kg) for 8 days. Liposomal 2c compound was solubilized to final concentration of 8-10 mg/mL in sterile 0.9% NaCl and injected *i.p.* daily (50 mg/kg) for 5 days. Immediately following treatment (*i.e.*, 5 or 8 days of drug injection) FACS profiles on cells isolated from mouse testes were performed to test if drug administration had deleterious effects on meiotic progression, and native ChIP for H4K12Ac, H4K16Ac or H3K9/14Ac histone acetylation marks, or H3K4Me3 and H3K27Me3 histone methylation marks, was performed to assess effects of treatment on histone mark profiles at meiotic hotspots. To verify effects of treatment on the levels of total acetylated-H3 and total acetylated-H4, westerns blots were performed on lysates from meiotic cells from the testes of treated animals. Briefly, meiotic cells isolated as described (20, 21) were washed once in PBS supplemented with protease inhibitors (protease inhibitor cocktail (Roche), 1 mM PMSF) and 10 mM Na-butyrate, resuspended in ARF buffer (50 mM HEPES, pH 7.5, 150 mM NaCl, 1 mM EDTA, 2.5 mM EGTA, 0.1% Tween-20) containing protease inhibitors and 10 mM Na-butyrate and lysed by sonication (Fisher Scientific, Sonic Dismembrator Model 100) for a few seconds at power level 2. Protein was quantified using

Micro BCA™ Protein Assay Kit (Thermo Scientific) and immunoblotted with 1:15000 of anti-acetyl-Histone H3 (Millipore, #06-599) or 1:2000 of anti-acetyl-Histone H3 (Active Motif, #39139), 1:1000 of anti-acetyl-Histone H4 (Active Motif, #39925), 1:2000 of anti-Histone H3 (Abcam, ab1791), 1:2000 of anti-Histone H4 (Abcam, ab10158) and 1:7000 of anti-β-Actin (Novus Biologicals, NB600-501) antibodies. Immune reactive bands were detected by enhanced chemiluminescence (Amersham Biosciences) or by Odyssey infrared imaging system (LI-COR Biosciences).

CO analysis after HDAC and HAT inhibitor treatment. CO rates for the *HS59.5* and *HS22* hotspots were determined 6 weeks after the last day of the drug injection. Sperm DNA was isolated from the epididymis of treated mice as described (24). As controls, sperm DNA from vehicle-only treated mice was isolated. CO analysis was performed following allele-specific PCR (24, 25). CO assays for treated sperm DNA at the *HS22* and *HS59.5* hotspots were run for DBA-to-B6 CO orientation using DNA samples from 3 independent treatments. Statistical significance in CO rates between treated and control samples were determined using Student's *t*-test. *HS59.5* ASOs were as described in Materials in Methods in *HS59.5* hotspot identification section above. *HS22* 5' allele specific primers were 22DBA-F1.1-1 (5'-ATG ACC CTC AAG GTC CTA C**C**-3') and 22DBA-F3.1-2 (5'-ATG GCC AGA CAC TGT AG**T**-3') for DBA, 22B6-F1.1-1 (5'-ATG ACC CTC AAG GTC CTA C**G**-3') and 22B6-F3.1-2 (5'-ATG GCC AGA CAC TGT AG**C**-3') for B6. The 3' primers were 22DBA- R7.1-1 (5'-TCG CCG ACT GAT GA**C**-3') and 22DBA-R6-2 (5'-GGC CGG CAT TTT AAT CTT CAT A**C**-3') for DBA and 22B6-R7.1-1 (5'-GCT CGC CGA CTG ATG A**T**-3') and 22B6-R6-2 (5'-GGC CGG CAT TTT AAT CTT CAT A**G**-3') for B6 (SNPs are indicated in bold font). The first round was performed using

294 the 22F1.1-1 and 22R7.1-1 primer pair (5.0 kb), and the second round with the 22F3.1-2
295 and 22R6-2 primer pair (4.6 kb). The first round of PCR reactions were performed at 94°C
296 for 1 min followed by 33 cycles at 94°C for 45 sec, 60°C for 45 sec, and 65°C for 5 min and
297 30 sec. The second round of PCR reactions were performed at 94°C for 1 min followed by
298 33 cycles at 94°C for 45 sec, and 62°C for 6 min. All primary PCR products were digested
299 with S1 nuclease to remove single-stranded DNA as described (24, 26). Secondary PCR
300 reactions were seeded with 100-fold diluted S1-treated DNA. Secondary PCR products
301 (70% of total reaction volume) were run on 0.8% agarose gels in 0.5 X TBE and visualized
302 with ethidium bromide and UV light. All the bands after the 2nd round of CO PCR were
303 sequenced using the Sequencher software (v4.9, GeneCodes) and recombinant molecules
304 were identified. *HS22* sequencing primers were HS22F1 (5'-TCT ATT GGC CTC GTA CCT
305 GTG-3'), HS22F2 (5'-AAC GGT GCC TTT ACC AAC AG-3'), HS22F3 (5'-GCT CTC ACA CAC CAC
306 CAC TTT-3'), HS22R0 (5'-GAT GAG TGG GAC TGG GAT ACA-3'), HS22R2 (5'-TCA GCT CAG
307 TGA GAA CCT AGT G-3'), and HS22R3 (5'-GAG AGC ATG ATG GGA ACA GAC-3').
308 Recombination rates and 95% confidence intervals were calculated as described (24, 25)
309 (Fig. 9B and D and Table A5 in the Appendices).
310
311 **Identification of PRDM9 binding motifs within the *HS22* hotspot.** To define putative
312 binding sites of PRDM9 within the *HS22* core, we scanned *HS22* C57Bl/6J sequence (24) for
313 a presence of short 15-mer consensus 9R motif specific for PRDM9 9R (C57Bl/6J) allele
314 (15) (see Fig. S4A) using 9R motif position weight matrix (PWM), which was kindly
315 provided by Dr. Pavel Khil, and MEME-ChIP software (http://meme.nbcr.net/meme/cgi-

bin/fimo.cgi). Statistical details and a list with obtained 9R motif sites for *HS22* core (9Rc1-9Rc7) are provided in Table A6 of the Appendices.

Accession numbers. Results of the microarray analysis and whole-genome data have been deposited in the Gene Expression Omnibus database under accession no. GSE57197 and no. GSEXXXX, respectively.

RESULTS

Expression analysis of genes encoding histone modification enzymes during meiosis I.

To initially assess possible dynamics of histone modifications in meiosis I, gene expression analysis was performed on highly FACS-purified populations of meiotic stage cells (20-22). Expression profiling and qRT-PCR analyses established differential gene expression of 11 histone acetyltransferases (HATs), 16 histone methyltransferases (HMTs) and 4 histone deacetylases and demethylases (HDACs and HDMTs) in early meiotic spermatogonia, pre-leptotene and leptotene/zygotene cells versus pachytene and later meiotic stage cells (Fig. 1; Tables A1 and A2, Appendices). Further, several of the HATs (*e.g.*, *Hat1*, *Ep300*, *Crebbp, Taf5*) and HMTs (*e.g.*, *Ash1l , Mll1, Prdm9, Suz12*) that are expressed at high levels during early meiosis I (Fig. 1A; Table A1, Appendices) target lysine residues of histones H3 and H4, and are essential for the transcription of meiotic genes, for germ cell and embryonic development, and/or for the DNA damage response (32-38). Finally, some

of the HAT and HMT encoding genes up-regulated at later stages of meiosis I (*e.g.*, *Kat5*, *Dot1l*, Fig. 1B; Table A1, Appendices) have functions in DSB repair (38, 39).

Dynamic regulation of histone H3 and H4 acetylation and methylation marks at recombination hotspot cores during meiosis I. The differential regulation of histone modifying enzymes suggested that histone marks might be dynamically controlled at hotspot cores prior to and/or following the formation of DSBs. To test this, we performed nChIP followed by real-time PCR analyses of several histone H3 and H4 acetylation and methylation marks in meiotic cells, from spermatogonia to diplotene, at four well-characterized meiotic recombination hotspots coined *HS22*, *HS59.4*, *HS59.5* and *HS61.1*, which are present on mouse chromosome 19 (Figs. 2-4; Fig. S1, and Fig. A1, Appendices) (10, 20, 24, 25). These four hotspots have crossover (CO) rates ranging from 0.05 to 6.0 x 10^{-4} per meiosis, which are comparable to the majority of mouse meiotic hotspots that have recombination frequencies of 10^{-5} to 10^{-3} (25, 40, 41).

Notably, ChIP analyses using validated antibodies to histone marks (presented as normalized profiles to no-antibody controls) revealed that active histone marks that are typical of open chromatin are a hallmark of hotspot cores in pre-leptotene cells, the stage of meiosis I immediately prior to the formation of DSBs (Figs. 2 and 3), a scenario that should facilitate access of these sites by the Spo11 endonuclease that directs DSBs at leptotene (14, 42). These include, for example, H4K12Ac and H3K4Me3 that have known roles in marking actively transcribed open chromatin regions (Fig. 2) (43, 44). Moreover, hotspot cores of pre-leptotene stage cells harbored several other histone modifications that are associated with open chromatin, including the acetylated H3K9Ac, H4K5Ac, H4K8Ac,

360 H4K12Ac, H4K16Ac and H4K91Ac marks (Fig. 3A), as well the active methylated marks
361 H3K4Me2, H3K36Me3 and H3K79Me1 (Fig. 3B) (44-46). Notably, there was concordance in
362 the overlap of the histone mark ChIP profiles with nucleosome occupancy maps, which
363 were determined by real-time PCR and whole genome sequencing (WGS) analyses of
364 micococcal-nuclease resistance regions across these fours hotspots (Fig. S2). Finally, in
365 some instances the activating histone marks were erased at hotspot cores in leptotene-
366 zygotene cells, and/or during later stages of meiosis (*e.g.*, pachytene-diplotene cells, Figs. 2
367 and 3; Fig. S1A).

368 Repressive histone methylation marks that are usually associated with
369 heterochromatic regions (H3K27Me3, H3K9Me3, H4K20Me1, H4K20Me2 and H4K20Me3)
370 (43, 44, 46, 47) were generally absent in hotspot cores in spermatogonia and pre-leptotene
371 stage cells (Fig. 4). Some repressive histone marks were evident at these cores during DSB
372 formation at leptotene-zygotene, and at later stages of meiosis (Fig. 4; Fig. S1B). However,
373 not all repressive histone marks followed this pattern. For example, H3K9Me3 and
374 H4K20Me3 marks were observed in pre-leptotene cells at the *HS59.4* and *HS22* cores,
375 respectively (Fig. 4). This could reflect the dual nature of these two histone marks, which
376 are present in both active and silenced genes (46, 48). Alternatively, the presence of such
377 repressive marks might correlate with the reduced recombination rates of some meiotic
378 hotspots, such as *HS59.4* (20).

379 Note that generally modest enrichment of histone modification marks detected by
380 nChIP at meiotic hotspot cores is an average of the entire meiotic population, and that this
381 only represents about 10% of the total of such marks, as only 10% of meiotic DSBs are
382 successfully repaired via CO events in mice (49, 50). These findings are consistent with the

genome-wide analysis of H3K4Me3 marks at mouse meiotic recombination hotspots (3), which showed that these marks are generally much weaker than the amplitude of H3K4Me3 signals found at transcription start sites.

Repressive histone H3 and H4 marks predominate at hotspot cores in inactive mouse backgrounds. To assess if changes in histone marks at a given hotspot core correlates with recombination activity of this hotspot, we compared the dynamics of these histone marks at the *HS22* hotspot during early meiosis I in the CAST/DBA strain, where this hotspot is inactive, versus in B6/DBA where *HS22* is active (24) (Fig. 5). Notably, the active acetylated and methylated histone marks H4K5Ac, H4K8Ac, H4K12Ac, and H3K4Me3 were depleted (Fig. 5A) at the *HS22* core in inactive CAST/DBA *vs.* B6/DBA spermatogonia, pre-leptotene and leptotene/zygotene stage cells. In contrast, the repressive H3K9Me3 and H3K27Me3 histone modifications were enriched at the *HS22* hotspot core in the inactive CAST/DBA versus B6/DBA early stage meiotic cells (Fig. 5B). Thus, histone marks typical of active, open chromatin at hotspot cores are indeed associated with the activity of meiotic recombination hotspots.

Chaotic histone marks are manifest at meiotic hotspots in *Spo11*$^{-/-}$ meiotic cells. In mouse *Spo11*$^{-/-}$ male spermatocytes DSBs are not generated, the chromosomes fail to synapse and meiosis arrests in prophase I prior to pachytene (51, 52). The pattern of histone modifications at hotspot cores in early *Spo11*$^{-/-}$ germ cells is chaotic, where both active and repressive marks are present (Fig. 6). For example, both active and repressive H3K4Me3 and H3K27Me3 histone methylated marks are present in early meiotic *Spo11*$^{-/-}$

406 cells at the *HS22* core and these accumulate to very high levels, up to a 23-27 fold increase
407 in *Spo11*$^{-/-}$ leptotene/zygotene-like stage cells *vs.* levels of these histone marks levels in
408 wild type early meiotic cells (Fig. 6A). Further, the active H4K12Ac mark is erased, and the
409 active H4K16Ac mark is enriched at the *HS22* hotspot core in pre-leptotene and
410 leptotene/zygotene *Spo11*$^{-/-}$ cells (Fig. 6B). Notably, expression patterns of genes encoding
411 histone acetylases, deacetylases, methylases and demethylases are very similar in early
412 stage meiotic cells from *Spo11*$^{-/-}$ and wild type mice (Fig. 7). Thus, Spo11 binding likely
413 contributes to and/or stabilizes an appropriate chromatin architecture at meiotic hotspot
414 cores, which promotes subsequent DSB formation.
415
416 **Histone acetylation is necessary for activating histone methylation marks at hotspot**
417 **cores and for meiotic recombination hotspot activity.** To test if histone acetylation
418 plays functional roles in the deposition of other histone marks at hotspots, and/or in
419 hotspot site selection, activity or CO resolution, we assessed the effects of *in vivo*
420 treatments with validated small molecule HDAC and HAT inhibitors (Figs. 8 and 9; Fig. S3).
421 As an HDAC inhibitor we used mercaptoacetamide "s2" (Fig. 8A, *left*), a broad spectrum
422 HDAC inhibitor (IC_{50} of 0.2 μM) (53) that was originally designed as anti-cancer drug and
423 that has prolonged activity *in vivo* (31). Treatment with s2 did not affect meiosis, as
424 reflected by FACS profiles (Fig. 8B, *left*), and led to expected increases in the total levels of
425 acetylated histone H3 in meiotic cells (Fig. 8C). Notably, s2 treatment (*vs.* vehicle)
426 significantly increased the levels of H4K16Ac and H3K9/14Ac marks (up to 18- and 14-
427 fold, respectively) at the hotspot cores tested (*HS22* and *HS59.5*) in spermatogonia, pre-
428 leptotene and leptotene-zygotene meiotic cells (Fig. 9A; Fig. S3A). Further, s2 treatment

429 also significantly increased (up to 6-fold) the levels of the active histone H3K4Me3 mark at
430 the *HS22* and *HS59.5* hotspot cores in these cells (Fig. 9A; Fig. S3A). Thus, increasing
431 histone acetylation marks also augments the deposition of histone methylation marks at
432 hotspot cores. Most importantly, increased histone acetylation marks at hotspot cores
433 correlated with marked increases in CO recombination rates at these hotspots, of up to 24-
434 and 15-fold for *HS59.5* and *HS22* hotspots, respectively (Fig. 9B; Table A5, Appendices).
435 Finally, s2 treatment also led to an increase of H4K12 acetylation at the inactive *HS22* core
436 in early meiosis I cells from CAST/DBA mice (Fig. S3B), but this did not activate hotspot
437 core activity in this strain (data not shown). Thus, deposition of histone acetylation marks
438 is not sufficient to initiate DSBs at meiotic hotspot cores in inactive strain backgrounds.
439 To test if histone acetylation is necessary for hotspot activity, mice were treated
440 with the cinnamoyl small molecule HAT inhibitor compound "2c" (Fig. 8A, *right*), which
441 inhibits p300 HAT activity (IC_{50} of 5 μM) and which blocks histone acetylase activity in
442 mammalian cells (28). For *in vivo* treatments we prepared liposome-encapsulated 2c drug
443 soluble in saline based on the protocol developed for curcumin (30). Treatment with
444 liposomal 2c had no toxicity for treated mice, had essentially no effect on meiotic
445 progression as judged by FACS analyses (Fig. 8B, *right*) yet led to, as expected, marked
446 reductions the levels of total acetylated histone H3 and H4 in meiotic cells (Fig. 8D).
447 Notably, 2c treatment essentially abolished histone H4K12Ac marks at *HS22* and *HS59.5*
448 recombination cores in spermatogonia, pre-leptotene and leptotene-zygotene meiotic
449 stages (Fig. 9C; Fig. S3C). Moreover, HAT inhibition also led to marked decreases in the
450 levels of the activating histone H3K4Me3 mark and to increases in the repressive histone
451 H3K27Me3 mark at the *HS22* and *HS59.5* cores (up to 10-fold) in early meiotic cells (Fig.

9C; Fig. S3C). Thus, histone acetylation controls the deposition of chromatin-activating and -repressing histone methylation marks at hotspot cores. Most importantly, hypoacetylation of histones H3 and H4 at hotspot cores was associated with marked reductions in CO rates, where recombination rates dropped 15-20 fold at *HS59.5* and *HS22* cores, respectively (Fig. 9D; Table A5, Appendices).

DISCUSSION

Roles of histone acetylation and methylation marks during mouse meiosis I. Many of histone modifying enzymes expressed in early meiotic cells (Fig. 1) are essential for mammalian development, where their deletion in the mouse leads to prenatal or postnatal lethality, defects in spermatogenesis, chromosomal aberrations and/or infertility (*e.g.*, deletion of *Hat1, Suv39h1/2, Suv4-20h1/2, Prdm9, Sirt1,* or *Sirt6)* (34, 35, 37, 54-58). Further, some of the histone acetylation and methylation marks targeted by these HATs and HMTs have known roles in mammalian germ cell development and meiosis. For example, mammalian germ cells, similar to embryonic stem cells, form bivalent (poised) chromatin domains that bear both activated H3K4Me3 and repressive H3K27Me3 histone marks at the promoters of a large set of developmental genes; this architecture appears important for maintenance of germ cell identity, and for the poised expression of regulators of somatic cells lineages (33, 59, 60). In addition, H3K9 and H3K4 methylation are required for higher order hetero- and eurochromatin structures needed for homologous chromosome synapsis and sex body formation (34, 35, 54). Finally, the H3K4Me3 mark is a known marker of meiotic DSBs in yeast and mammals and appears to function in activating meiotic gene transcription (14, 35).

Dynamic control of select histone acetylation and methylation marks at recombination hotspot cores during meiosis I. The data reported herein establish that, unlike nucleosome occupancy (10, 20), histone marks at hotspot cores are dynamic. First, histone acetylation and methylation marks typical of open chromatin are present at hotspot cores at meiotic stages that precede the formation the DSB by Spo11 and that would be predicted to facilitate Spo11 binding and cleavage. Accordingly, at these early stages of meiosis there is a dearth of repressive histone methylation marks at hotspot cores. Later in meiosis, several of the active histone marks appear to be erased and repressive marks then often appear. Second, activating histone marks are not found at hotspot cores in strains where these hotspots are inactive, which are rather decorated by repressive histone marks. Collectively, these findings suggest an open chromatin environment is necessary for meiotic DSBs. However, as shown in our HDAC inhibitor *in vivo* studies, the deposition of activating histone acetylation is not sufficient to confer activity to an otherwise inactive hotspot core.

Profiling a cast of histone marks revealed that select modifications have distinct dynamics at hotspot cores. For example, acetylated histone H4 at K5, K8, K12 and K16 are enriched at hotspot cores in spermatogonia and pre-leptotene stages, prior to the formation of DSB, and then decrease at leptone-zygotene cells and are nearly fully erased following DSB repair in pachytene-diplotene cells (Figs. 2 and 3A; Fig. S1A). In contrast, the histone H3K9Ac mark increases from spermatogonia to diplotene, and histone H4K91Ac is enriched both at pre-leptotene and pachytene-diplotene cells, but is depleted in leptotene-zygotene cells (Fig. 3A). In part, these differences may reflect specific functions of such modified histones during the formation or repair of meiotic DSB. Indeed, H4K91

acetylation plays essential functions in the chromatin assembly and DNA damage repair (61). Further, the changes in histone acetylation marks at hotspots noted herein have corollaries in yeast, where during HO endonuclease-mediated recombination, which resembles Spo11-induced events (62), histone H4 (K5, K8, K12 and K16) acetylated marks accumulate at the sites flanking the DSB followed by deacetylation of these marks during DSB repair (63). Notably, several histone acetyltransferases (Hat1p, Gcn5, Esa1) and histone deacetylases (Rpd3, Sir2 and Hst1) are recruited to DSBs during homologous recombination repair (36, 63).

The H4K4Me3 mark is a known hallmark of mouse and human meiotic hotspots that is deposited by the meiotic-specific histone methyltransferase PRDM9 (14). Profiling revealed that the active H3K4Me2, H3K36Me3, H3K79Me1 marks, as well as the repressive H4K20Me3 mark, are also enriched at *HS22* hotspot in pre-leptotene meiotic cells, just prior to the formation of DSBs (Figs. 3B and 4B). H3K79Me1 and H4K20Me3 marks were also present at *HS22* core at leptotene-zygotene meiotic stages and enhanced at pachytene-diplotene cells (Figs. 3B and 4B). Notably, the H3K79 and H4K20 marks have been linked to the recruitment of the DNA repair factor 53BP1 to DNA damage sites in response to UV-irradiation in mice and yeast (38), and thus it is feasible they might play similar roles in DNA repair in meiosis.

Generally, active acetylated and methylated histone marks are reduced, and repressive methylated marks are increased, at hotspot cores in leptotene–zygotene and/or pachytene-diplotene cells, right after the formation of DSBs (Figs. 2-4; Fig. S1). This suggests a resetting of chromatin conformation after the DSB is formed and then repaired.

In accord with this notion, both H3K4Me3 and H3K27Me3 marks, featuring bivalent chromatin regions, are enriched at meiotic recombination hotspots in human sperm (64).

Spo11 is necessary for proper chromatin structure at mouse recombination hotspots. In the absence of DSBs in *Spo11*$^{-/-}$ mice, a presumably bivalent-like chromatin structure is formed that has both active (H3K4Me3) and repressive (H3K27Me3) histone methylation marks at hotspot cores of pre-leptotene and leptotene-zygotene-like stage cells (Fig. 6A). Further, some histone acetylation marks are depleted (H4K12Ac at pre-leptotene and leptotene-zygotene-like stages) or enriched (H4K16Ac, at all three meiotic stages) at recombination hotspot cores in *Spo11*$^{-/-}$ mice (Fig. 6B). As the expression of HATs/HDACs and HMT/HDMTs genes is similar in *Spo11*$^{-/-}$ and wild-type early stage meiotic cells (Fig. 7), this suggests that Spo11 itself, alone or in complex with chromatin binding factors, contributes to the organization of hotspot cores and is required to initiate and/or sustain specific histone marks at DSBs.

Histone acetylation is necessary, but not sufficient, for mouse meiotic hotspot activity. Notably, our *in vivo* HAT and HDAC inhibitor studies revealed instructive roles for histone acetylation in controlling meiotic hotspots. First, inhibition of HDACs augmented histone acetylation marks at *HS22* and *HS59.5* hotspot cores in spermatogonia, pre-leptotene and leptotene-zygotene meiotic cells and also, surprisingly, led to increases in activating histone methylation marks at these sites, for example of H3K4Me3 (Fig. 9A; Fig. S3A). Conversely, inhibition of HATs abolished histone acetylation and histone methylation marks typical of open chromatin, and rather led to the accumulation of repressive histone

543 methylation marks (*e.g.*, H3K27Me3) at *HS22* and *HS59.5* hotspot cores in early meiotic
544 cells (Fig. 9C; Fig. S3C). These effects suggest the need for histone acetylation to initiate or
545 sustain an open chromatin structure at hotspots that is necessary for subsequent histone
546 methylation, and hotspot activity. Alternatively, this could reflect hierarchical histone
547 modifications at recombination hotspot cores. We favor the former alternative, whereby
548 histone acetylation at hostpot cores facilitates the deposition of activating histone
549 methylation marks (*e.g.*, via PRDM9) that then fully opens chromatin to allow access of the
550 protein recombination machinery and cleavage by Spo11. Indeed, HDAC inhibitor
551 treatment augments levels of the H4K16Ac mark at meiotic hotspot cores (Fig. 9A; Fig.
552 S3A), and H4K16Ac has known roles in disrupting the compaction of higher order
553 chromatin domains (65). In addition, s2 treatment also augments H3K9 and K14 marks
554 acetylation at meiotic hotspot cores in early meiotic cells (Fig. 9A; Fig. S3A), and H3K9Ac
555 and H3K14 Ac have known roles in allowing access of the repair machinery to damaged
556 DNA (38).

557 Notably, our studies revealed that manipulating histone acetylation levels at hotspot
558 cores leads to concordant, and profound, changes in hotspot activity (Fig. 9B and D; Table
559 A5, Appendices). We propose that the opening of chromatin at meiotic hotspots by histone
560 acetylation at stages that precede the DSB will increase the accessibility of protein
561 recombination machinery to the core and stimulate first the DSB event (*e.g.,* PRDM9,
562 followed by Spo11) and eventually CO formation at these sites (Fig. 9B; Table A5,
563 Appendices). In contrast, compaction of chromatin at recombination cores by blocking of
564 histone acetylation restricts access of PRDM9 and Spo11 to meiotic hotspots, which leads
565 to a decrease in the frequency of DSBs and to marked reductions in hotspot activity (Fig.

9D; Table A5, Appendices). Our findings strongly support the notion that histone acetylation is necessary for meiotic recombination, and they are consistent with analyses of epigenetic mutant strains of yeast and plants that have shown associated changes in hotspot activity (9, 66-68). For example, deletion of the *S. pombe* HAT *Gcn5,* which directs hyperacetylation of the *ade6-M26* hotspot, leads to reductions in DSBs and CO rates at this hotspot (9). Conversely, deletion of the *S. cerevisiae* HDAC *Rpd3* augments *HIS4* hotspot activity (67). However, our HDAC inhibitor studies in CAST/DBA mouse strain where *HS22* hotspot is inactive have also shown that augmenting histone acetylation (Fig. S3B) is not sufficient to confer recombinogenic activity. Thus, other levels of control in addition to histone acetylation marks must also be manifest in licensing hotspot cores for DSB cleavage and recombination.

Collectively, the data establish a dynamic role for histone modifications in controlling the activity and resolution of mammalian recombination hotspots. Specifically, these studies reveal instructive roles for acetylated histones at mouse recombination hotspot cores, where acetylated histones are revealed as necessary, but not sufficient, for imbuing hotspot activity. The data support a model (Fig. 10; Fig. S4, and Table A6, Appendices) where initially inactive condensed chromatin that is present at hotspots cores in early germ cells; *e.g.*, primordial germ cells (32, 69, 70), shifts to an open conformation at the onset of meiosis in spermatagonia and pre-leptotene stage cells, and suggest that open chromatin is driven, at least in part, by the deposition of acetylated marks on histones H3 (K9) and H4 (K5, K8, K12, K16 and K91) by histone acetyltransferases expressed at these cells (Figs. 1A and 10; Fig. S4B). In turn, acetylation of histone H3 and H4 tails opens up chromatin at the hotspot core, which makes them more accessible for the binding of

PRDM9, followed by PRDM9-driven deposition of H3K4Me3 marks at histones at these sites and for the deposition of additional histone H3 active methylated marks (H3K4Me2, H3K36Me3 and H3K79Me1) by HMTs expressed in early meiotic stage cells (Figs. 1B and 10; Fig. S4B). Collectively, this creates a chromatin environs conducive to Spo11 binding and the initiation of meiotic recombination (Fig. 10). Thus, histone acetylation, along with PRDM9, controls mammalian recombination hotspot site selection.

FUNDING INFORMATION

This project was supported in part by funding from the State of Florida to Scripps Florida (to P. R. J. B.) and the Moffitt Cancer Center (to J. L. C.), by monies from the Marie Mayer and PGA Women's Cancer Awareness Days Postdoctoral Fellowships in Cancer Biology (to I. V. G.), by grant R01GM085079 from the National Institute of General Medical Sciences (to P. R. J. B. and J. L. C.), and by the Cancer Center Support Grant P30 CA076292 to the Moffitt Cancer Center from the National Cancer Institute (to J. L. C.). The funders had no role in study design, data collection and interpretation, or the decision to submit the work for publication.

ACKNOWLEDGMENTS

We are indebted to Drs. Pavel Khil (NIDDK/NIH) and Matthew Pipkin (Scripps Florida) for reviewing the manuscript, to Dr. Howard Petrie, Bivian Torres and Kimberley Lowe (Scripps Florida flow cytometry core), Brandon Young and Bradley Long (Scripps Florida Genomics Core) for their technical advice and assistance, and to numerous colleagues for

611 discussions and insights. We also thank Dr. R. Daniel Camerini-Otero (NIDDK/NIH) for
612 providing *Spo11*$^{-/-}$ mice.

613

614 **Conflict of interest**

615 The authors declare that they have no conflict of interest.
616

REFERENCES

1. **Wahls WP, Davidson MK.** 2010. Discrete DNA sites regulate global distribution of meiotic recombination. Trends Genet **26:**202-208.
2. **Buard J, Barthes P, Grey C, de Massy B.** 2009. Distinct histone modifications define initiation and repair of meiotic recombination in the mouse. EMBO Journal **28:**2616-2624.
3. **Smagulova F, Gregoretti IV, Brick K, Khil P, Camerini-Otero RD, Petukhova GV.** 2011. Genome-wide analysis reveals novel molecular features of mouse recombination hotspots. Nature **472:**375-378.
4. **Qiao H, Prasada Rao HB, Yang Y, Fong JH, Cloutier JM, Deacon DC, Nagel KE, Swartz RK, Strong E, Halloway JK, Cohen PE, Schimenti J, Ward J, Hunter N.** 2014. Antagonistic roles of ubiquitin ligase HEI10 and SUMO ligase RNF212 regulate meiotic recombination. Nat Genet **46:**194-199.
5. **Hirota K, Mizuno K, Shibata T, Ohta K.** 2008. Distinct chromatin modulators regulate the formation of accessible and repressive chromatin at the fission yeast recombination hotspot ade6-M26. Molecular Biology of the Cell **19:**1162-1173.
6. **Yamashita K, Shinohara M, Shinohara A.** 2004. Rad6-Bre1-mediated histone H2B ubiquitylation modulates the formation of double-strand breaks during meiosis. Proc Natl Acad Sci U S A **101:**11380-11385.
7. **Sollier J, Lin W, Soustelle C, Suhre K, Nicolas A, Geli V, de La Roche Saint-Andre C.** 2004. Set1 is required for meiotic S-phase onset, double-strand break formation and middle gene expression. EMBO Journal **23:**1957-1967.
8. **Youds J, Boulton SJ.** 2011. The choice in meiosis - defining the factors that influence crossover or non-crossover formation. J Cell Sci **124:**201-213.

9. **Yamada T, Mizuno K, Hirota K, Kon N, Wahls WP, Hartsuiker E, Murofushi H, Shibata T, Ohta K.** 2004. Roles of histone acetylation and chromatin remodeling factor in a meiotic recombination hotspot. EMBO J **23:**1792-1803.

10. **Getun IV, Wu ZK, Bois PRJ.** 2012. Organization and roles of nucleosomes at mouse meiotic recombination hotspots. Nucleus **3:**244-250.

11. **Wagner CR, Kuervers L, Baillie DL, Yanowitz JL.** 2010. xnd-1 regulates the global recombination landscape in Caenorhabditis elegans. Nature **467:**839-843.

12. **Mieczkowski PA, Dominska M, Buck MJ, Lieb JD, Petes TD.** 2007. Loss of a histone deacetylase dramatically alters the genomic distribution of Spo11p-catalyzed DNA breaks in Saccharomyces cerevisiae. Proc Natl Acad Sci U S A **104:**3955-3960.

13. **Borde V, Robine N, Lin W, Bonfils S, Geli V, Nicolas A.** 2009. Histone H3 lysine 4 trimethylation marks meiotic recombination initiation sites. EMBO Journal **28:**99-111.

14. **Baudat F, Imai Y, de Massy B.** 2013. Meiotic recombination in mammals: localization and regulation. Nat Rev Genet **14:**794-806.

15. **Brick K, Smagulova F, Khil P, Camerini-Otero RD, Petukhova GV.** 2012. Genetic recombination is directed away from functional genomic elements in mice. Nature **485:**642-645.

16. **Baudat F, Buard J, Grey C, Fledel-Alon A, Ober C, Przeworski M, Coop G, de Massy B.** 2010. PRDM9 Is a Major Determinant of Meiotic Recombination Hotspots in Humans and Mice. Science **327:**836-840.

17. **Parvanov ED, Petkov PM, Paigen K.** 2010. Prdm9 controls activation of mammalian recombination hotspots. Science **327:**835.

18. **Grey C, Barthes P, Chauveau-Le Friec G, Langa F, Baudat F, De Massy B.** 2011. Mouse PRDM9 DNA-binding specificity determines sites of histone H3 lysine 4 trimethylation for initiation of meiotic recombination. PLoS Biol **9:**e1001176.

19. **Baker CL, Walker M, Kajita S, Petkov PM, Paigen K.** 2014. PRDM9 binding organizes hotspot nucleosomes and limits Holliday junction migration. Genome Res **24:**724-732.

20. **Getun IV, Wu ZK, Khalil AM, Bois PR.** 2010. Nucleosome occupancy landscape and dynamics at mouse recombination hotspots. EMBO Rep **11:**555-560.

21. **Getun IV, Torres B, Bois PR.** 2011. Flow cytometry purification of mouse meiotic cells. J Vis Exp **50:**pii: 2602.

22. **Fallahi M, Getun IV, Wu ZK, Bois PRJ.** 2010. A global expression switch marks pachytene initiation during mouse male meiosis. Genes **1:**469-483.

23. **Okada Y, Scott G, Ray MK, Mishina Y, Zhang Y.** 2007. Histone demethylase JHDM2A is critical for Tnp1 and Prm1 transcription and spermatogenesis. Nature **450:**119-123.

24. **Bois PR.** 2007. A Highly Polymorphic Meiotic Recombination Mouse Hotspot Exhibits Incomplete Repair. Mol Cell Biol **27:**7053-7062.

25. **Wu ZK, Getun IV, Bois PR.** 2010. Anatomy of mouse recombination hot spots. Nucleic Acids Research **38:**2346-2354.

26. **Kauppi L, May CA, Jeffreys AJ.** 2009. Analysis of meiotic recombination products from human sperm. Methods Mol Biol **557:**323-355.

27. **Kozikowski AP, Chen Y, Gaysin A, Chen B, D'Annibale MA, Suto CM, Langley BC.** 2007. Functional differences in epigenetic modulators-superiority of mercaptoacetamide-based histone deacetylase inhibitors relative to hydroxamates in cortical neuron neuroprotection studies. J Med Chem **50:**3054-3061.

28. **Costi R, Di Santo R, Artico M, Miele G, Valentini P, Novellino E, Cereseto A.** 2007. Cinnamoyl compounds as simple molecules that inhibit p300 histone acetyltransferase. J Med Chem **50:**1973-1977.

29. **Wang D, Veena MS, Stevenson K, Tang C, Ho B, Suh JD, Duarte VM, Faull KF, Mehta K, Srivatsan ES, Wang MB.** 2008. Liposome-encapsulated curcumin suppresses growth of head

and neck squamous cell carcinoma in vitro and in xenografts through the inhibition of nuclear factor kappaB by an AKT-independent pathway. Clin Cancer Res **14:**6228-6236.

30. **Li L, Braiteh FS, Kurzrock R.** 2005. Liposome-encapsulated curcumin: in vitro and in vivo effects on proliferation, apoptosis, signaling, and angiogenesis. Cancer **104:**1322-1331.
31. **Konsoula Z, Cao H, Velena A, Jung M.** 2009. Pharmacokinetics-pharmacodynamics and antitumor activity of mercaptoacetamide-based histone deacetylase inhibitors. Mol Cancer Ther **8:**2844-2851.
32. **Kota SK, Feil R.** 2010. Epigenetic transitions in germ cell development and meiosis. Dev Cell **19:**675-686.
33. **Chen T, Dent SY.** 2014. Chromatin modifiers and remodellers: regulators of cellular differentiation. Nat Rev Genet **15:**93-106.
34. **Godmann M, Lambort R, Kimmins S.** 2009. The dynamic epigenetic program in male germ cells: Its role in spermatogenesis, testis cancer, and its response to the environment. Microsc Res TEch **72:**603-619.
35. **Hayashi S, Yoshida K, Matsui Y.** 2005. A histone H3 methyltransferase controls epigenetic events required for meiotic prophase. Nature **438:**374-378.
36. **Qin S, Parthun MR.** 2006. Recruitment of the type B histone acetyltransferase Hat1p to chromatin is linked to DNA double-strand breaks. Mol Cell Biol **26:**3649-3658.
37. **Nagarajan R, Ge Z, Sirbu B, Doughty C, Garcia PA, Schlederer M, Annunziato AT, Cortez D, Kenner L, Parthun MR.** 2013. Histone acetyl transferase 1 is essential for mammalian development, genome stability, and the processing of newly synthesized histones H3 and H4. PLoS Genet **9:**e1003518.
38. **Dinant C, Houtsmuller AB, Vermeulen W.** 2008. Chromatin structure and DNA damage repair. Epigenetics Chromatin **1:**9.

39. **Tang J, Cho NW, Cui G, Manion EM, Shanbhag NM, Botuyan MV, Mer G, Greenberg RA.** 2013. Acetylation limits 53BP1 association with damaged chromatin to promote homologous recombination. Nat Struct Mol Biol **20:**317-325.

40. **Guillon H, Baudat F, Grey C, Liskay RM, de Massy B.** 2005. Crossover and noncrossover pathways in mouse meiosis. Mol Cell **20:**563-573.

41. **Paigen K, Petkov P.** 2010. Mammalian recombination hot spots: properties, control and evolution. Nat Rev Genet **11:**221-233.

42. **Keeney S.** 2008. Spo11 and the formation of DNA double-strand breaks in meiosis. Genome Dyn Stab **2:**81-123.

43. **Shones DE, Zhao K.** 2008. Genome-wide approaches to studying chromatin modifications. Nat Rev Genet **9:**179-191.

44. **Wang Z, Zang C, Rosenfeld JA, Schones DE, Barski A, Cuddapah S, Cui K, Roh T-Y, Peng W, Zhang MQ, Zhao K.** 2008. Combinatorial patterns of histone acetylations and methylations in the human genome. Nat Genet **40:**897-903.

45. **Steger DJ, Lefterova MI, Ying L, Stonestorm AJ, Schupp M, Zhuo D, Vakoc AL, Kim JE, Chen J, Lazar MA, Biobel GA, R. VC.** 2008. DOT1L/KMT4 Recruitment and H3K79 methylation are ubiquitouslycoupled with gene transcription in mammalian cells. Mol Cell Biol **28:**2825-2839.

46. **Barski A, Cuddapah S, Cui K, Roh TY, Schones DE, Wang Z, Wei G, Chepelev I, Zhao K.** 2007. High-resolution profiling of histone methylations in the human genome. Cell **129:**823-837.

47. **Karachentsev D, Sarma K, Reinberg D, Steward R.** 2005. PR-Set7-dependent methylation of histone H4 Lys 20 functions in repression of gene expression and is essential for mitosis. Genes Dev **19:**431-435.

48. **Squazzo SL, O'Geen H, Komashko VM, Krig SR, Jin VX, Jang SW, Margueron R, Reinberg D, Green R, Farnham PJ.** 2006. Suz12 binds to silenced regions of the genome in a cell-type-specific manner. Genome Res **16:**890-900.

49. **Cole F, Kauppi L, Lange J, Roig I, Wang R, Keeney S, Jasin M.** 2012. Homeostatic control of recombination is implemented progressively in mouse meiosis. Nat Cell Biol **14:**424-430.

50. **Kauppi L, Jasin M, Keeney S.** 2013. How much is enough? Control of DNA double-strand break numbers in mouse meiosis. Cell Cycle **12:**2719-2720.

51. **Romanienko PJ, Camerini-Otero RD.** 2000. The mouse Spo11 gene is required for meiotic chromosome synapsis. Mol Cell **6:**975-987.

52. **Bellani MA, Romanienko PJ, Cairatti DA, Camerini-Otero RD.** 2005. SPO11 is required for sex-body formation, and Spo11 heterozygosity rescues the prophase arrest of Atm-/- spermatocytes. J Cell Sci **118:**3233-3245.

53. **Konsoula R, Jung M.** 2008. In vitro plasma stability, permeability and solubility of mercaptoacetamide histone deacetylase inhibitors. Int J Pharm **361:**19-25.

54. **Peters AH, O'Carroll D, Scherthan H, Mechtler K, Sauer S, Schöfer C, Weipoltshammer K, Pagani M, Lachner M, Kohlmaier A, Opravil S, Doyle M, Sibilia M, Jenuwein T.** 2001. Loss of the Suv39h histone methyltransferases impairs mammalian heterochromatin and genome stability. Cell **107:**323-337.

55. **Schotta G, Sengupta R, Kubicek S, Malin S, Kauer M, Callén E, Celeste A, Pagani M, Opravil S, Rosa-Velazquez IA, Espejo A, Bedford MT, Nussenzweig A, Busslinger M, Jenuwein T.** 2008. A chromatin-wide transition to H4K20 monomethylation impairs genome integrity and programmed DNA rearrangements in the mouse. Genes Dev **22:**2048-2061.

56. **Yu BD, Hess JL, Horning SE, Brown GA, Korsmeyer SJ.** 1995. Altered Hox expression and segmental identity in Mll-mutant mice. Nature **378:**505-508.

57. **Ayton P, Sneddon SF, Palmer DB, Rosewell IR, Owen MJ, Young B, Presley R, Subramanian V.** 2001. Truncation of the Mll gene in exon 5 by gene targeting leads to early preimplantation lethality of homozygous embryos. Genesis **30:**201-212.

58. **Toiber D, Erdel F, Bouzoune K, Silberman DM, Zhong L, Mulligan P, Sebastian C, Cosentino C, Martinez-Pastor B, Giacosa S, D'Urso A, Näär AM, Kingston R, Rippe K, Mostoslavsky R.** 2013. SIRT6 recruits SNF2H to DNA break sites, preventing genomic instability through chromatin remodeling. Mol Cell **51:**454-468.

59. **Lesch BJ, Dokshin GA, Young RA, McCarrey JR, Page DC.** 2013. A set of genes critical to development is epigenetically poised in mouse germ cells from fetal stages through completion of meiosis. Proc Natl Acad Sci U S A **110:**16061-16066.

60. **Lesch BJ, Page DC.** 2014. Poised chromatin in the mammalian germ line. Development **141:**3619-3626.

61. **Ye J, Ai X, Eugeni EE, Zhang L, Carpenter LR, Jelinek MA, Freitas MA, Parthun MR.** 2005. Histone H4 lysine 91 acetylation a core domain modification associated with chromatin assembly. Mol Cell **18:**123-130.

62. **Malkova A, Klein F, Leung W-Y, Haber JE.** 2000. HO endonuclease-induced recombination in yeast meiosis resembles Spo11-induced events. Proc Natl Acad Sci U S A **97:**14500-14505.

63. **Tamburini BA, Tyler JK.** 2005. Localized histone acetylation and deacetylation triggered by the homologous recombination pathway of double-strand DNA repair. Mol Cell Biol **25:**4903-4913.

64. **Zeng J, Yi SV.** 2014. Specific modifications of histone tails, but not DNA methylation, mirror the temporal variation of mammalian recombination hotspots. Genome Biol Evol **6:**2918-2929.

65. **Shogren-Knaak M, Ishi H, Sun JM, Pazin MJ, Davie JR, Peterson CL.** 2006. Histone H4-K16 acetylation controls chromatin structure and protein interactions. Science **311:**844-847.

66. **Perrella G, Consiglio MF, Aiese-Cigliano R, Cremona G, Sanchez-Moran E, Barra L, Errico A, Bressan RA, Franklin FC, Conicella C.** 2010. Histone hyperacetylation affects meiotic recombination and chromosome segregation in Arabidopsis. Plant J **62:**796-806.

67. **Merker JD, Dominska M, Greenwell PW, Rinella E, Bouck DC, Shibata Y, Strahl BD, Mieczkowski P, Petes TD.** 2008. The histone methylase Set2p and the histone deacetylase Rpd3p repress meiotic recombination at the HIS4 meiotic recombination hotspot in Saccharomyces cerevisiae. DNA Repair (Amst) **7:**1298-1308.

68. **Yelina NE, Choi K, Chelysheva L, Macaulay M, de Snoo B, Wijnker E, Miller N, Drouaud J, Grelon M, Copenhaver GP, Mezard C, Kelly KA, Henderson IR.** 2012. Epigenetic remodeling of meiotic crossover frequency in Arabidopsis thaliana DNA methyltransferase mutants. PLoS Genet **8:**e1002844.

69. **Sasaki H, Matsui Y.** 2008. Epigenetic events in mammalian germ-cell development: reprogramming and beyond. Nat Rev Genet **9:**129-140.

70. **De Felici M.** 2011. Nuclear reprogramming in mouse primordial germ cells: epigenetic contribution. Stem Cells Int**:**425863.

71. **Nightingale KP, Baumann M, Eberharter A, Mamais A, Becker PB, Boyes J.** 2007. Acetylation increases access of remodelling complexes to their nucleosome targets to enhance initiation of V(D)J recombination. Nucleic Acids Res **35:**6311-6321.

72. **Wysocka J, Swigut T, Xiao H, Milne TA, Kwon SY, Landry J, Kauer M, Tackett AJ, Chait BT, Badenhorst P, Wu C, Allis D.** 2006. A PHD finger of NURF couples histone H3 lysine 4 trimethylation with chromatin remodelling. Nature **442:**86-90.

Figure Legends

FIG 1 Expression of histone-modifying enzymes during meiosis. (A) Profiling of differentially expressed genes encoding histone acetylases and deacetylases in all meiosis I stages isolated via FACS from wild-type B6/DBA mouse testes. (B) Profiling of differentially expressed genes encoding histone methylases and demethylases in all meiosis I stages isolated via FACS from wild-type B6/DBA mouse testes. In all heatmaps an absolute fold change filter of 1.5-fold for spermatogonia/average pachytene expression ratio was applied to obtain differentially expressed genes followed by hierarchical clustering. (A and B) Only significantly changed probe sets with *p*-value (corrected) <0.05 are shown. Microarray data were normalized across the median for all wild-type and *Spo11*$^{-/-}$ (see Fig. 7) samples. Microarray analysis is described in Materials and Methods. Details of statistical analysis are provided in Table A1 of the Appendices and findings were confirmed by qRT-PCR (Fig. 1C and 1D). (C) qRT-PCR analyses of genes encoding HATs and HDACs was performed for all stages of meiosis I. The *y*-axis scale shows normalized expression ratio in the indicated meiotic stage versus expression in spermatogonia. (D) qRT-PCR analyses for specific meiotic stage marker genes that are selectively expressed at different stages of meiosis I (23). (C and D) Results are the means and s.e.m. for technical replicates (n=3). qRT-PCR analyses details are described in Materials and Methods. Real-time PCR primers pairs used in (C) are shown in Table A2 of the Appendices.

FIG 2 Profiles of active histone marks at mouse meiotic recombination hotspots in early meiotic prophase. Representative normalized native ChIP profiles of the active H4K12Ac and H3K4Me3 histone marks are shown at *HS22*, *HS59.4, HS59.5* and *HS61.1* hotspots in spermatogonia, pre-leptotene and leptotene-zygotene meiotic cells. Normalized native ChIP profiles were obtained from real-time PCR data analysis for validated primer pairs that overlap these hotspots (see Materials and Methods, Fig. A1 in the Appendices). The *y*-axis scale indicates the normalized ratios of bound native ChIP fractions of a given histone mark versus no antibody control. The *x*-axis represents the location across the analyzed *HS* locus. Initial native ChIP profiles were obtained by calculating an absolute fold enrichment between bound and input ChIP DNA fractions, using the $2^{-\Delta Ct}$ formula. Each of the ChIP profiles shown is the average of three independent, normalized ChIP experiments. Red shading indicates the hotspot cores. The horizontal red line between pre-leptotene and leptotene-zygotene meiotic stages indicates the stage when Spo11 generates DSBs.

FIG 3 Profiles of active acetylated and methylated histone marks at *HS22* hotspot in early meiotic prophase. (A) Representative normalized native ChIP profiles of the active acetylated H3K9Ac, H4K5Ac, H4K8Ac, H4K16Ac and H4K91Ac histone marks are shown at spermatogonia, pre-leptotene, leptotene-zygotene and pachytene-diplotene meiotic stage cells for the *HS22* hotspot. (B) Representative normalized native ChIP profiles of the active methylated H3K4Me2, H3K36Me3 and H3K79Me1 histone marks are shown at spermatogonia, pre-leptotene, leptotene-zygotene and pachytene-diplotene meiotic stage cells for the *HS22* hotspot. Normalized histone modification profiles in (A) and (B) were obtained as in Fig. 2 legend. ChIP profiles shown are the average of three independent,

855 normalized ChIP experiments. Hotspot cores, red shading; horizontal red line, stage when
856 Spo11 generates DSBs.
857
858 **FIG 4** Profiles of repressive histone methylated marks at mouse meiotic recombination
859 hotspots in early meiotic prophase. (A) Representative normalized native ChIP profiles of
860 the repressive H3K27Me3 and H3K9Me3 histone methylated marks are shown at *HS22,*
861 *HS59.4, HS59.5* and *HS61.1* hotspots in spermatogonia, pre-leptotene and leptotene-
862 zygotene meiotic stage cells. (B) Additional representative normalized native ChIP profiles
863 of the repressive H4K20Me1, H4K20Me2, and H4K20Me3 histone methylated marks are
864 shown at the *HS22* hotspot in spermatogonia, pre-leptotene, leptotene-zygotene and
865 pachytene-diplotene meiotic stage cells. Normalized histone modification profiles in (A)
866 and (B) were obtained as in Fig. 2 legend. ChIP profiles shown are the average of three
867 independent, normalized ChIP experiments. Hotspot cores, red shading; horizontal red line,
868 stage when Spo11 generates DSBs.
869
870 **FIG 5** Profiles of active acetylated and methylated H3 and H4 histone marks at the *HS22*
871 hotspot in inactive versus active genetic backgrounds. (A) Normalized ratios of bound
872 native ChIP fractions of active acetylated H4K5Ac, H4K8Ac, H4K12Ac and methylated
873 H3K4Me3 histone marks at the *HS22* hotspot core in the inactive CAST/DBA strain versus
874 the active B6/DBA mouse strain for spermatogonia, pre-leptotene and leptotene-zygotene
875 meiotic stage cells. (B) Normalized ratios of bound native ChIP fractions of repressive
876 methylated H3K9Me3 and H3K27Me3 histone marks at the *HS22* hotspot core in the
877 inactive CAST/DBA strain versus the active B6/DBA strain for spermatogonia, pre-

878 leptotene and leptotene-zygotene meiotic stage cells. Inactive *HS22* hotspot cores in (A)
879 and (B) are indicated with blue shading. Normalization was performed as described in
880 Materials and Methods. Data shown are the average of three independent, normalized ChIP
881 experiments.
882
883 **FIG 6** Profiles of active and repressive histone H3 and H4 marks in *Spo11*$^{-/-}$ versus wild-
884 type genetic background at the *HS22* hotspot. (A) Normalized ratios of bound native ChIP
885 fractions of active and repressive histone methylated (H3K4Me3 and H3K27Me3) marks at
886 the *HS22* hotspot were determined in spermatogonia, pre-leptotene and leptotene-
887 zygotene-like meiotic stage cells from *Spo11*$^{-/-}$ versus wild-type B6/DBA mice. (B)
888 Normalized ratios of bound native ChIP fractions of active histone acetylated (H4K12Ac
889 and H4K16Ac) marks at the *HS22* hotspot were determined in spermatogonia, pre-
890 leptotene and leptotene-zygotene-like meiotic stage cells from *Spo11*$^{-/-}$ versus wild-type
891 B6/DBA mice. Hotspot cores found in B6/DBA mice are indicated with red shading in (A)
892 and (B). Normalization method is described in Materials and Methods. Data shown are the
893 average of at least two independent, normalized ChIP experiments.
894
895 **FIG 7** Expression of genes encoding histone modifying enzymes in early meiotic cells from
896 *Spo11*$^{-/-}$ mice. (A) Profiling of differentially expressed genes encoding histone acetylases
897 and deacetylases in spermatogonia, pre-leptotene and leptotene-zygotene-like meiotic
898 stages isolated via FACS from *Spo11*$^{-/-}$ mouse testes. (B) Profiling of differentially expressed
899 genes encoding histone methylases and demethylases in spermatogonia, pre-leptotene and
900 leptotene-zygotene-like meiotic stages isolated via FACS from *Spo11*$^{-/-}$ mouse testes. For

comparison purposes, expression of histone-modifying enzymes in three *Spo11*$^{-/-}$ (*left*) and respective wild-type B6/DBA (*right*) meiosis I stage cells is shown in each of the heatmaps in (A) and (B). In all heatmaps an absolute fold change filter of 1.5-fold for spermatogonia/average pachytene expression ratio from wild type mice (see Fig. 1) was applied to obtain the differentially expressed gene list followed by hierarchical clustering. Only significantly changed probe sets with p-value (corrected) <0.05 are shown. Microarray data were normalized across the median for the wild type (Fig. 1) and *Spo11*$^{-/-}$ heatmaps. Microarray analysis is described in Materials and Methods. Details of statistical analysis are provided in Table A1 of the Appendices.

FIG 8 Effects of HDAC and HAT inhibitors on meiotic cell distribution and global levels of acetylated histones. (A) Structures of the HDAC inhibitor s2 (*left*) and the HAT inhibitor 2c (*right*) are shown. (B) *Top panels*, FACS profiles were performed on meiotic cells isolated from the testes of drug- and vehicle-treated mice to assess potential effects on meiosis. Mice were treated with the HDAC inhibitor s2 or vehicle (*left panels)*, or with the HAT inhibitor 2c or vehicle (*right panels)*, meiotic cells were isolated and analyzed by FACS. *Bottom tables*, percentages of each population in vehicle and inhibitor treated mice. Sp – Spermatogonia, pL – pre-Leptotene, L/Z – Leptotene-Zygotene, P/D – Pachytene-Diplotene. (C) Effects of the HDAC inhibitor s2 on the total levels of acetylated histone H3 in meiotic cells. Male mice were treated with the s2 compound, meiotic cells were isolated and levels of Ac-H3 and total H3 were determined by immunoblot analyses. (D) Effects of the HAT inhibitor 2c on the total levels of acetylated histone H3 and H4. Mice were treated with the 2c compound, meiotic cells were isolated and levels of Ac-H3, Ac-H4, total H3 and total H4

924 were determined by immunoblot analyses. (C and D) Equal loading was confirmed by
925 immunoblotting with antibody to β-actin.
926
927 **FIG 9** Histone acetylation controls the activity of mouse meiotic recombination hotspots.
928 (A) Normalized native ChIP analyses of active acetylated H4K16Ac, H3K9/14Ac and
929 methylated H3K4Me3 histone marks were performed for the *HS22* hotspot in
930 spermatogonia, pre-leptotene and leptotene-zygotene stage cells from 10-week old
931 B6/DBA mice treated *i.p.* with the HDAC inhibitor s2 (see Fig. 8, A and B, *left*) versus
932 vehicle. Red shading indicates the s2-activated *HS22* hotspot core. (B) CO rates for s2-
933 treated (blue bars) *vs.* vehicle treated (red bars) sperm samples at the *HS59.5* and *HS22*
934 hotspots. (C) Normalized native ChIP analyses of active acetylated H4K12Ac and
935 methylated H3K4Me3 and inactive methylated H3K27Me3 histone marks were performed
936 for the *HS22* hotspot in spermatogonia, pre-leptotene and leptotene-zygotene stage cells
937 from 10-week old B6/DBA mice treated *i.p.* with the HAT inhibitor 2c (see Fig. 8, A and B,
938 *right*) versus vehicle. Blue shading indicates the 2c-inactivated *HS22* hotspot core. (D) CO
939 rates for 2c-treated (blue bars) *vs.* vehicle treated (red bars) sperm samples at the *HS59.5*
940 and *HS22* hotspots. Normalization method and inhibitor treatment details for (A) and (C)
941 are described in Materials and Methods. Data shown are the average of at least two
942 independent, normalized ChIP experiments. (B and D) Results are the means and s.e.m. for
943 biological replicates (n = 3); Student's t-test, *, $p<0.05$.
944
945 **FIG 10** A proposed model for meiotic recombination hotspot activation by histone
946 acetylation. *Top*, a condensed chromatin structure is proposed to be manifest at the *HS22*

hotspot core in early germ cells (EGC), as represented by three central closely juxtaposed nucleosomes at the core (black and grey circles). Potential PRDM9 binding sites (red vertical lines) are positioned next to "black" nucleosomes (see Fig. S4A and Table A6 in the Appendices). *Middle top*, licensing hotspots cores for activation occurs in spermatogonia (Sp) and pre-leptotene (pL) meiotic cells, which requires deposition of acetylated marks on histones H3 and H4 that are directed by HATs that are expressed in these cells (Fig. 1A; Fig. S4B). This leads to the formation of open chromatin, which is likely facilitated by binding of chromatin remodeling factors (CRMFs) to histone acetylated tails (1, 33, 71). *Middle bottom*, acetylated open chromatin (red nucleosomes) then allows PRDM9 binding at its cognate binding sequences (cyan vertical lines), followed by deposition of H3K4Me3 marks by PRDM9, as well as the deposition of other histone H3 active methylated marks by HMTs that are expressed in these cells (Fig. 1B; Fig. S4B). *Bottom*, DNA regions juxtaposed to active "red" nucleosome sites then become accessible for DSB cleavage by Spo11 at leptotene (L), which appears to occur via the recruitment of chromatin binding proteins (ChBP) to H3K4Me3 tails (18, 33, 72). DSBs are then repaired by meiotic recombination machinery leading to a CO, or to gene conversion without a CO (NCO).

Getun *et al.* Figure 1

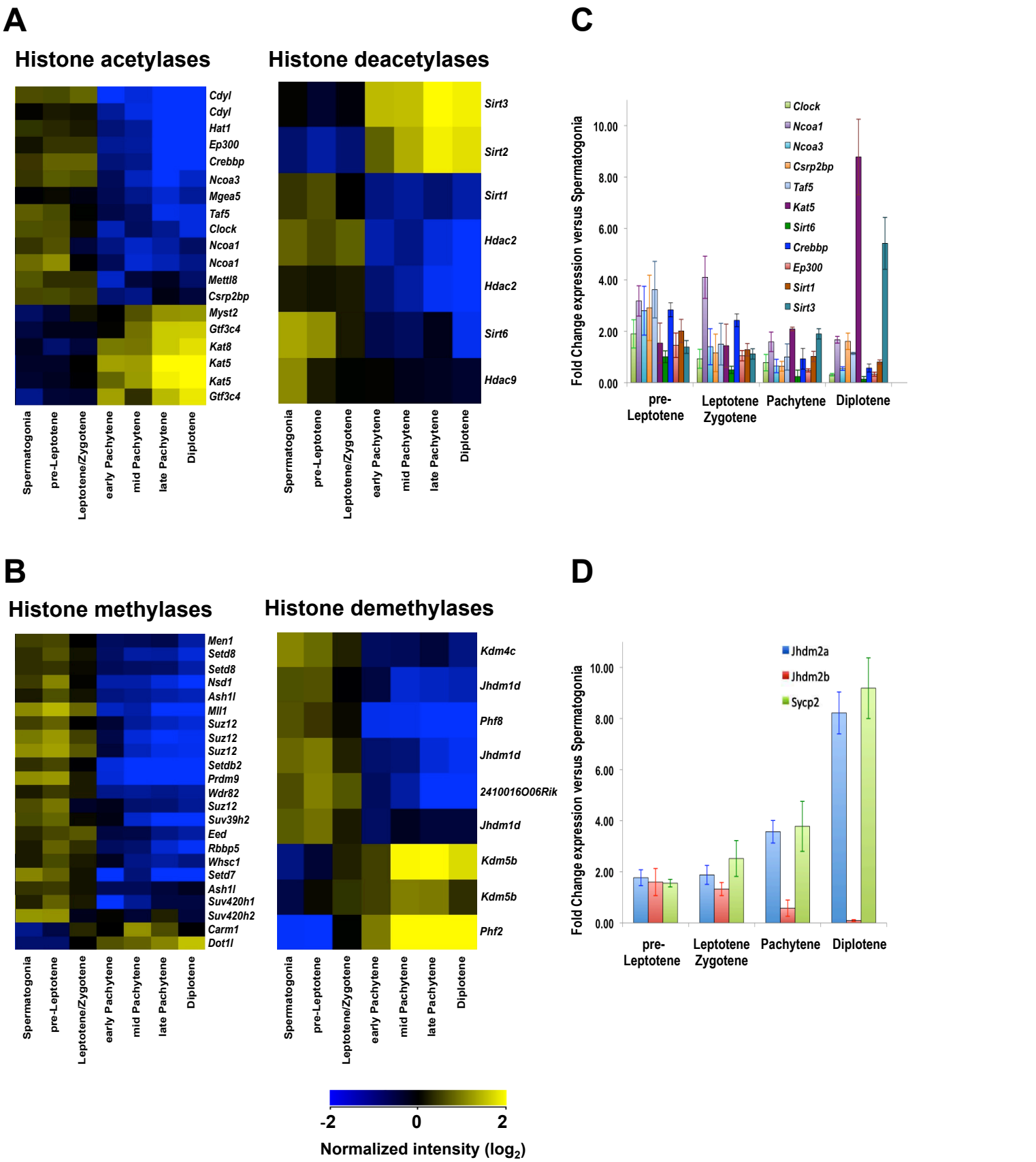

Getun *et al.* Figure 2

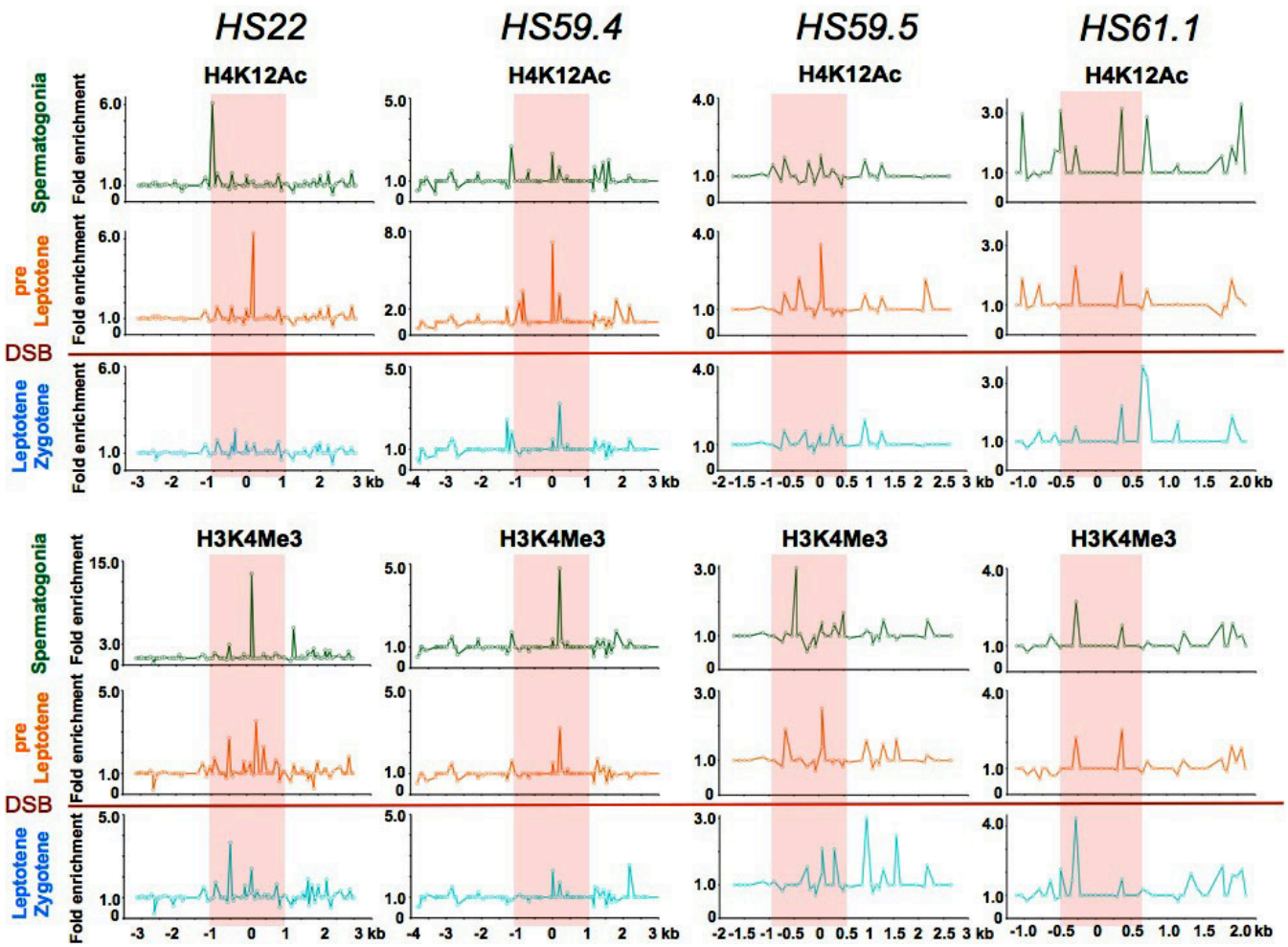

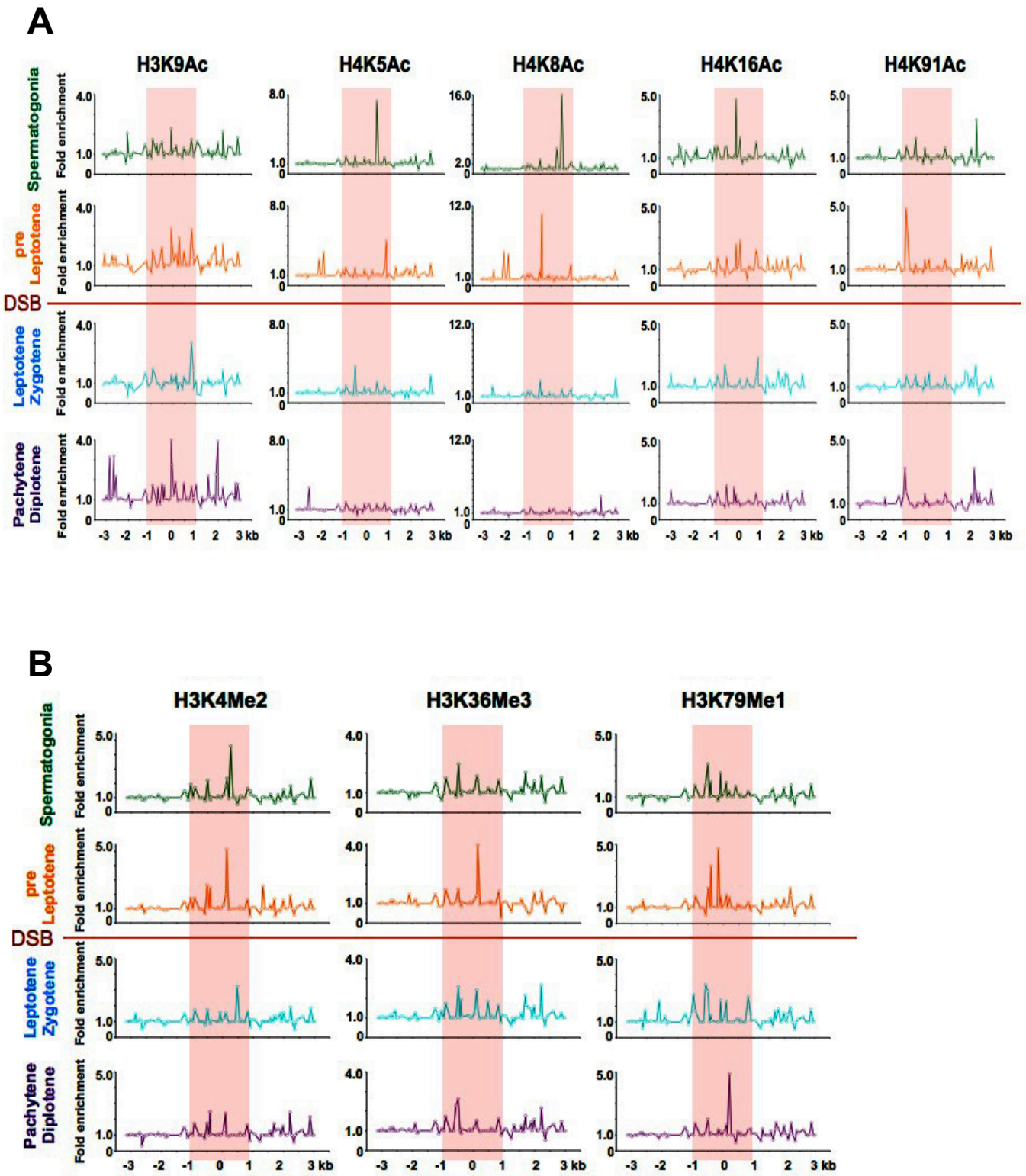
A
H3K9Ac
H4K5Ac
H4K8Ac
H4K16Ac
H4K91Ac
Spermatogonia
pre Leptotene
DSB
Leptotene Zygotene
Pachytene Diplotene
Fold enrichment
-3 -2 -1 0 1 2 3 kb
B
H3K4Me2
H3K36Me3
H3K79Me1
Spermatogonia
pre Leptotene
DSB
Leptotene Zygotene
Pachytene Diplotene
Fold enrichment
-3 -2 -1 0 1 2 3 kb

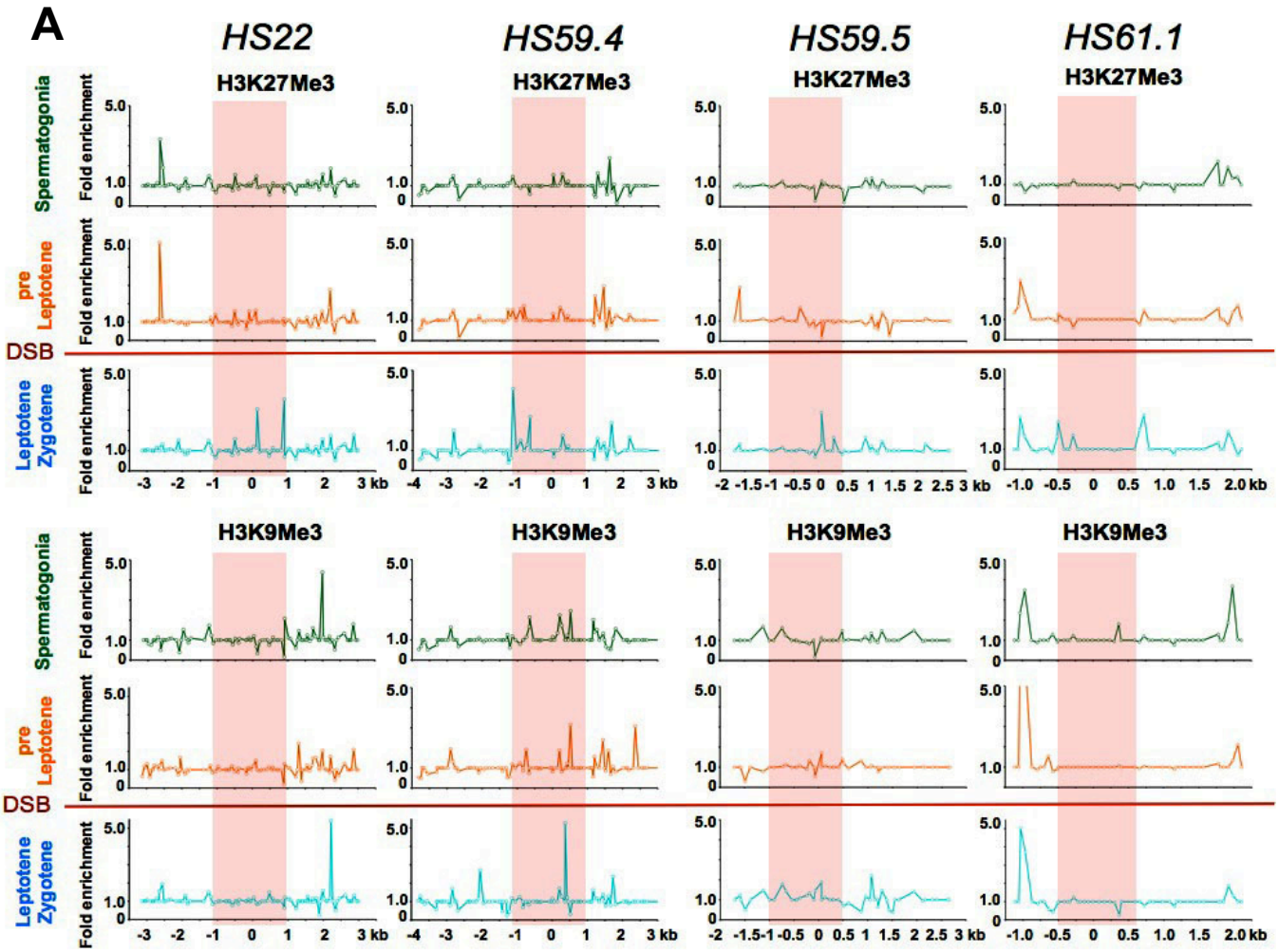
A
HS22
HS59.4
HS59.5
HS61.1
H3K27Me3
H3K9Me3
Spermatogonia
pre Leptotene
DSB
Leptotene Zygotene
Fold enrichment
5.0
1.0
0
-3 -2 -1 0 1 2 3 kb
-4 -3 -2 -1 0 1 2 3 kb
-2 -1.5 -1 -0.5 0 0.5 1 1.5 2 2.5 3 kb
-1.0 -0.5 0 0.5 1.0 1.5 2.0 kb

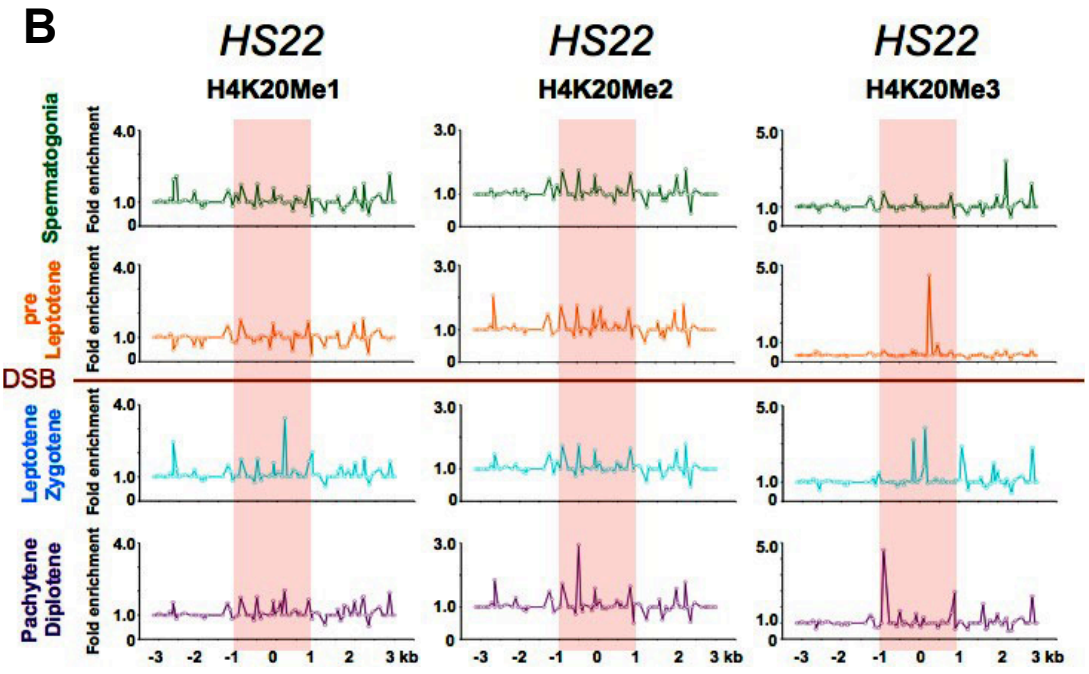
B
HS22
HS22
HS22
H4K20Me1
H4K20Me2
H4K20Me3
Spermatogonia
pre Leptotene
DSB
Leptotene Zygotene
Pachytene Diplotene
Fold enrichment
4.0
3.0
5.0
1.0
0
-3 -2 -1 0 1 2 3 kb

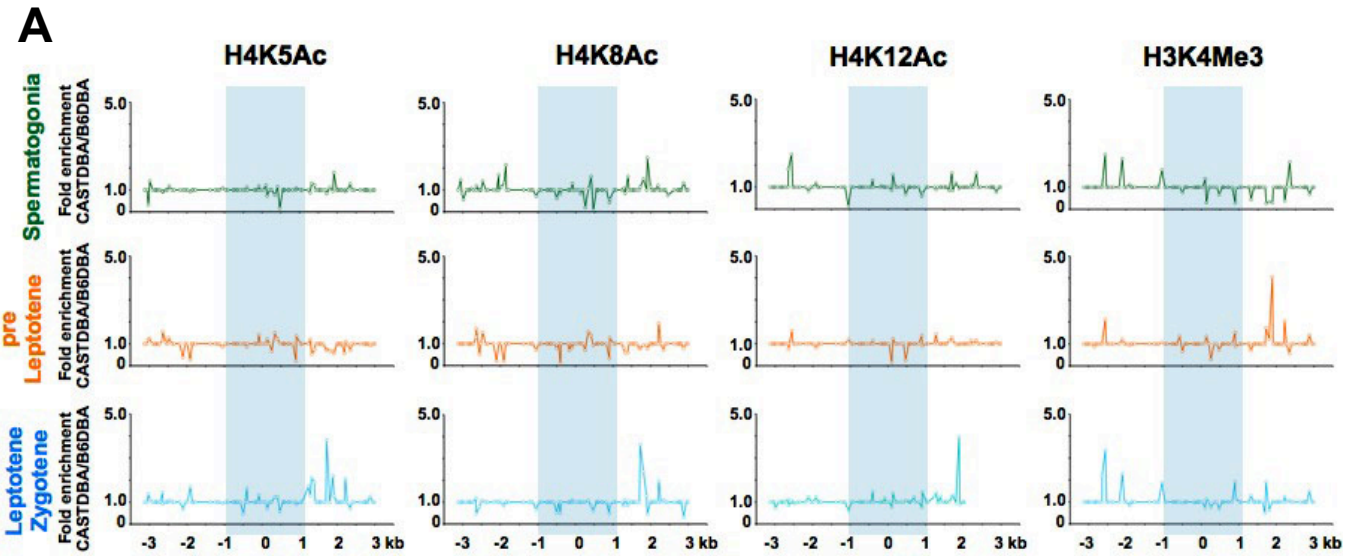
A
H4K5Ac
H4K8Ac
H4K12Ac
H3K4Me3
Spermatogonia
pre Leptotene
Leptotene Zygotene
Fold enrichment CASTDBA/B6DBA
5.0
1.0
0
-3 -2 -1 0 1 2 3 kb

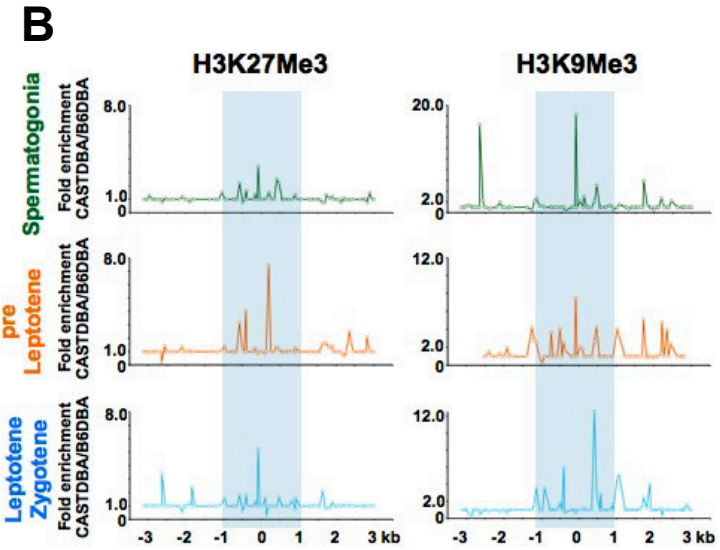
B
H3K27Me3
H3K9Me3
Spermatogonia
pre Leptotene
Leptotene Zygotene
Fold enrichment CASTDBA/B6DBA
8.0
20.0
12.0
2.0
1.0
0
-3 -2 -1 0 1 2 3 kb

A

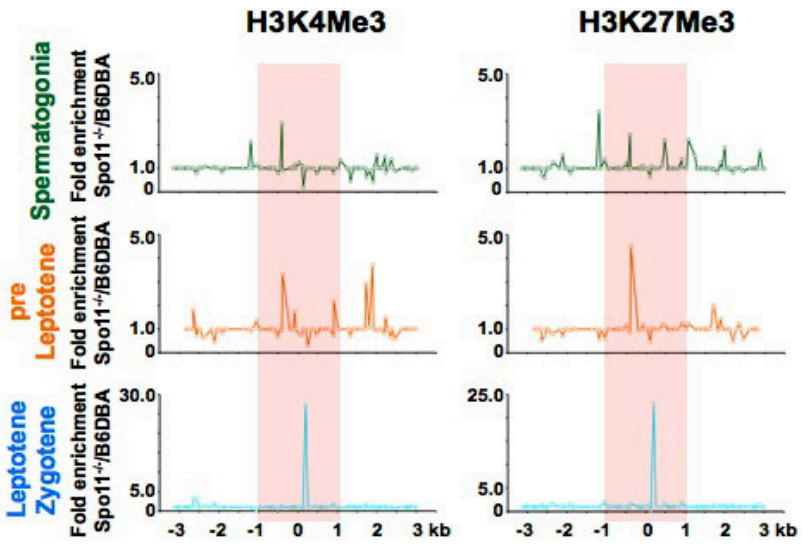
H3K4Me3
H3K27Me3
Spermatogonia
pre Leptotene
Leptotene Zygotene
Fold enrichment Spo11-/-/B6DBA
5.0
1.0
0
30.0
25.0
-3 -2 -1 0 1 2 3 kb

B

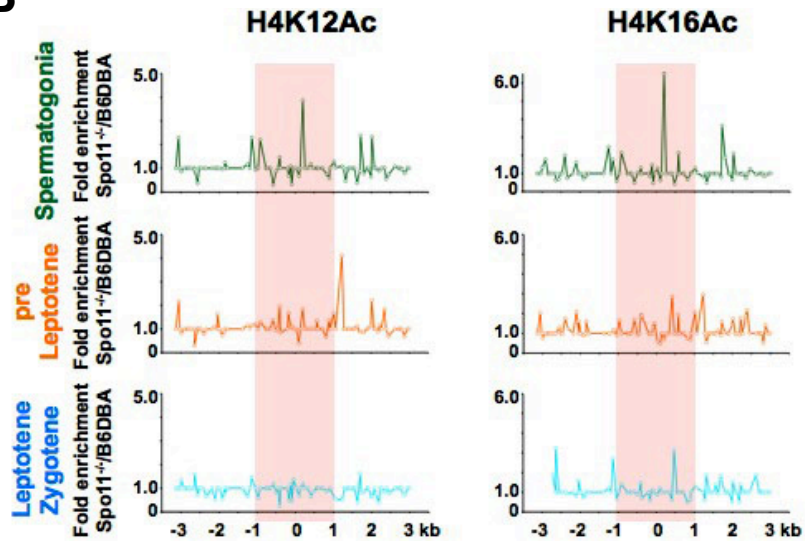
H4K12Ac
H4K16Ac
Spermatogonia
pre Leptotene
Leptotene Zygotene
Fold enrichment Spo11-/-/B6DBA
5.0
6.0
1.0
0
-3 -2 -1 0 1 2 3 kb

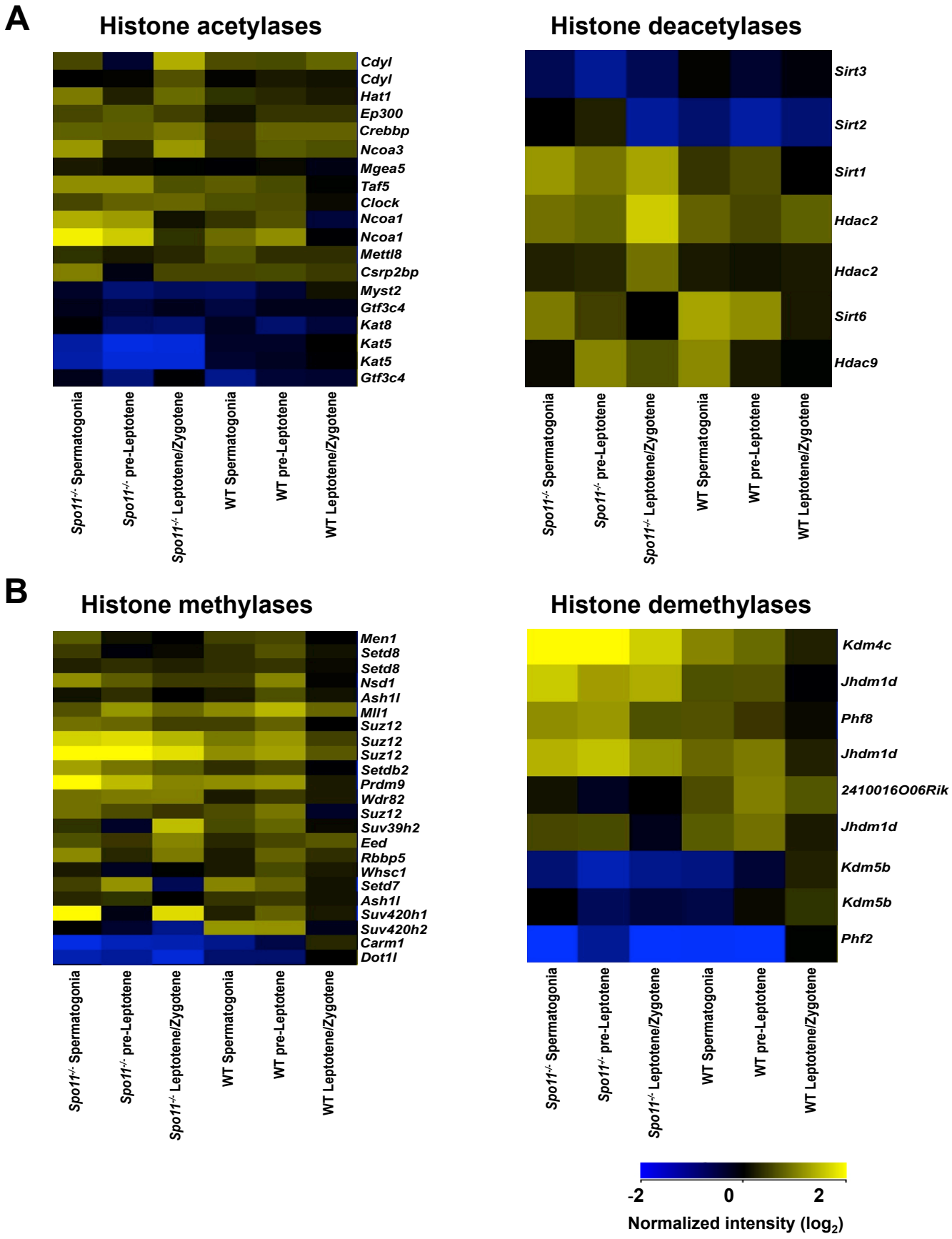
A
Histone acetylases
Cdyl
Cdyl
Hat1
Ep300
Crebbp
Ncoa3
Mgea5
Taf5
Clock
Ncoa1
Ncoa1
Mettl8
Csrp2bp
Myst2
Gtf3c4
Kat8
Kat5
Kat5
Gtf3c4
Spo11-/- Spermatogonia
Spo11-/- pre-Leptotene
Spo11-/- Leptotene/Zygotene
WT Spermatogonia
WT pre-Leptotene
WT Leptotene/Zygotene
Histone deacetylases
Sirt3
Sirt2
Sirt1
Hdac2
Hdac2
Sirt6
Hdac9
Spo11-/- Spermatogonia
Spo11-/- pre-Leptotene
Spo11-/- Leptotene/Zygotene
WT Spermatogonia
WT pre-Leptotene
WT Leptotene/Zygotene
B
Histone methylases
Men1
Setd8
Setd8
Nsd1
Ash1l
Mll1
Suz12
Suz12
Suz12
Setdb2
Prdm9
Wdr82
Suz12
Suv39h2
Eed
Rbbp5
Whsc1
Setd7
Ash1l
Suv420h1
Suv420h2
Carm1
Dot1l
Spo11-/- Spermatogonia
Spo11-/- pre-Leptotene
Spo11-/- Leptotene/Zygotene
WT Spermatogonia
WT pre-Leptotene
WT Leptotene/Zygotene
Histone demethylases
Kdm4c
Jhdm1d
Phf8
Jhdm1d
2410016O06Rik
Jhdm1d
Kdm5b
Kdm5b
Phf2
Spo11-/- Spermatogonia
Spo11-/- pre-Leptotene
Spo11-/- Leptotene/Zygotene
WT Spermatogonia
WT pre-Leptotene
WT Leptotene/Zygotene
-2
0
2
Normalized intensity (log2)

Getun *et al.* Figure 8

A

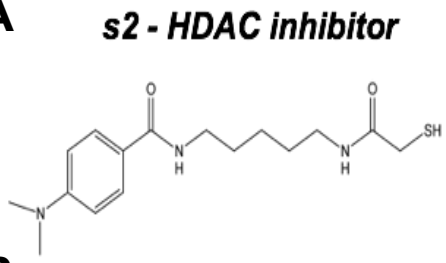

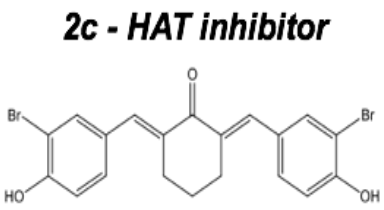

B

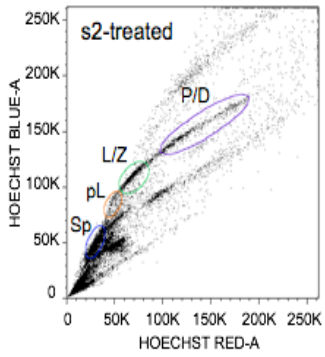

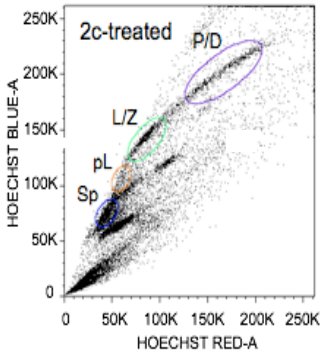

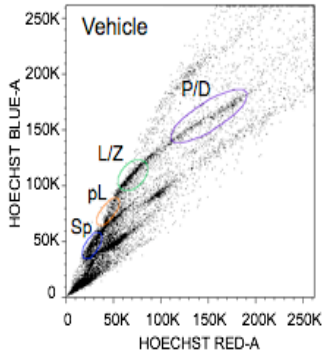

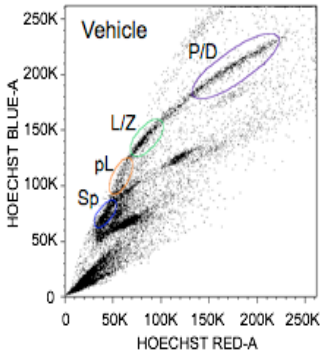

C

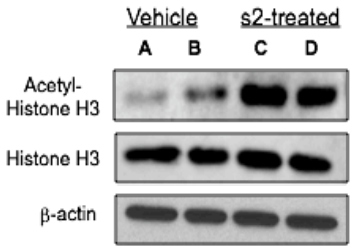

A, B - DMSO/saline vehicle
C, D - treated mice

D

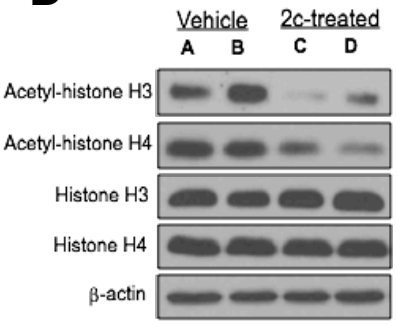

A, B - empty liposome vehicle
C, D - treated mice

	s2-treated Population, %	Vehicle Population, %
Sp	24.4	28.3
pL	9.0	12.1
L/Z	40.9	35.0
P/D	25.7	24.6

	2c-treated Population, %	Vehicle Population, %
Sp	21.9	22.8
pL	10.0	11.9
L/Z	33.0	27.6
P/D	35.1	37.7

Getun *et al.* Figure 9

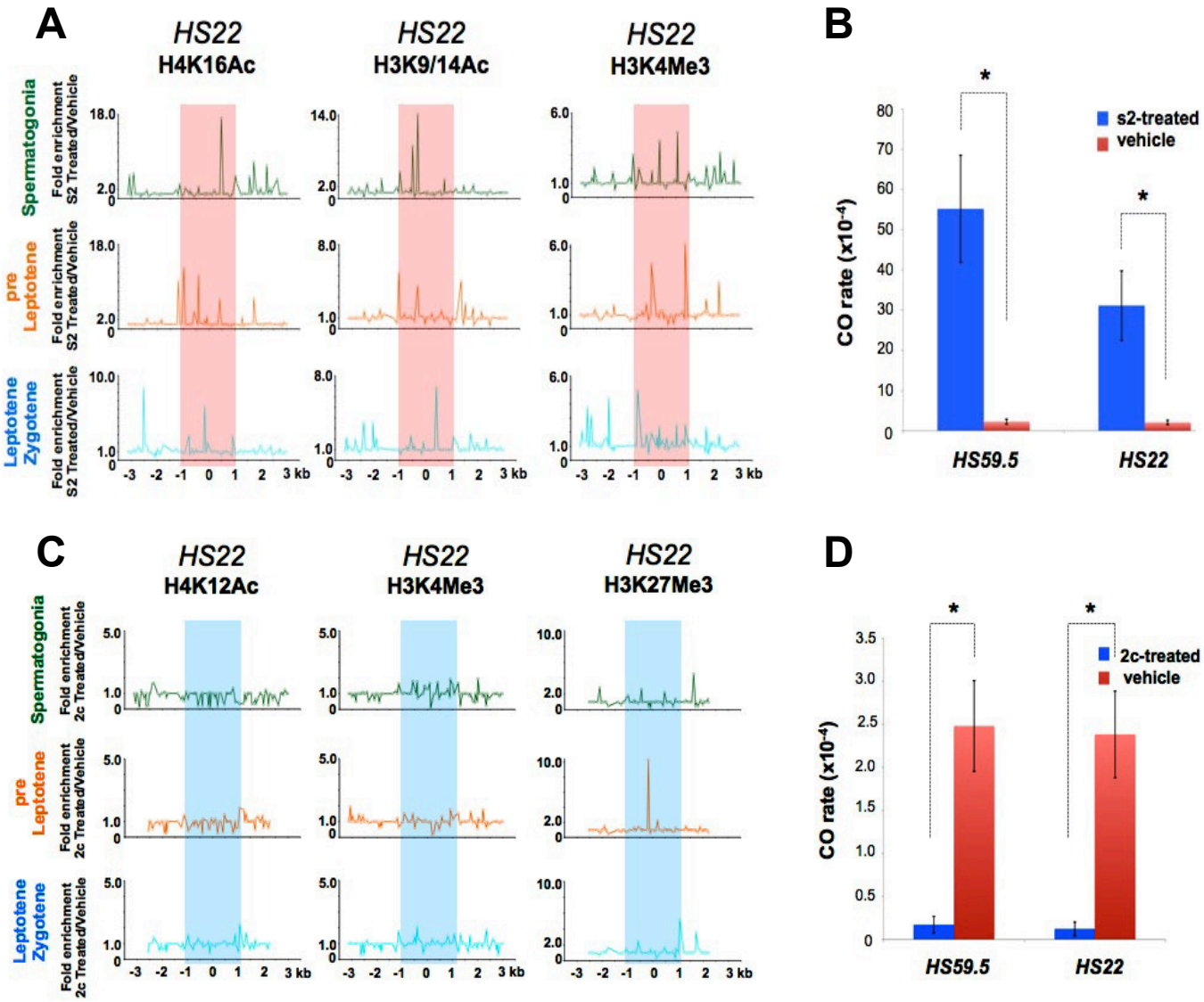

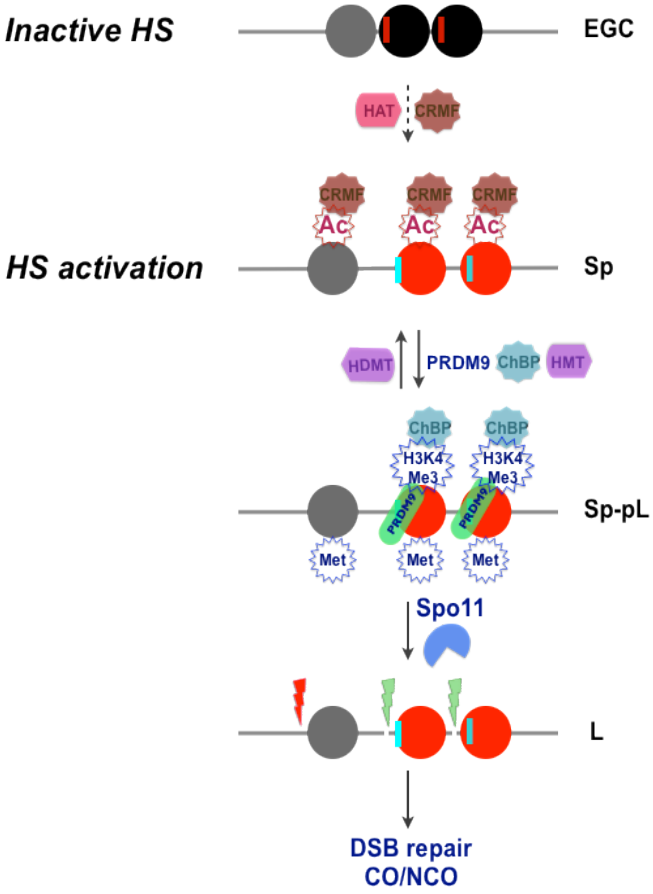
Inactive HS
EGC
HAT
CRMF
HS activation
CRMF
Ac
Sp
HDMT
PRDM9
ChBP
HMT
H3K4
Me3
Met
Sp-pL
Spo11
L
DSB repair
CO/NCO